Regulators of the breast tumor immune microenvironment: PD-L1 and regulatory T cells

by

Yeni Romero

B.A., Kansas State University, 2018

A THESIS

submitted in partial fulfillment of the requirements for the degree

MASTER OF SCIENCE

Department of Biochemistry and Molecular Biophysics
College of Arts and Sciences

KANSAS STATE UNIVERSITY
Manhattan, Kansas

2020

Approved by:

Major Professor
Anna Zolkiewska

Copyright

© Yeni Romero 2020.

Abstract

Tumors consist of a diverse population of cancer cells as well as various tumor-infiltrating immune cells, soluble factors, and extracellular matrix proteins, which are collectively known as the tumor immune microenvironment (TIME). The interactions between cancer cells and their microenvironment heavily influence tumor progression and therapeutic responses, often leading to tumor immune evasion and therapeutic resistance. Understanding these complex interactions will help develop novel strategies to target tumor cells or improve the efficacy of existing therapies. The goal of my research was to explore the role of two regulators of the tumor immune microenvironment, PD-L1 and regulatory T cells, in triple negative breast cancer (TNBC).

Programmed death-ligand 1 (PD-L1) is a negative regulator of the immune system that acts as a “brake” to keep the body’s immune responses under control. However, in cancer, PD-L1 expression leads to immune evasion and poor disease outcomes. In breast cancer, PD-L1 expression is most upregulated in the TNBC subtype. Under certain circumstances, transmembrane PD-L1 can be cleaved, generating a soluble form containing an intact receptor-binding domain. In my research, I investigated the cleavage of PD-L1 expressed on the surface of tumor cells. I found that a ~37-kDa N-terminal cleavage product of PD-L1 is released to the culture media. Analysis of the ~18-kDa C-terminal PD-L1 fragment demonstrated that this fragment is unstable and readily eliminated by lysosomal degradation. Furthermore, I identified ADAM10 and ADAM17, two members of the cell surface family of ADAM metalloproteases, as mediators of the cleavage of transmembrane PD-L1.

Regulatory T cells (Tregs) are a subset of T cells that play a role in regulating or suppressing other immune cells. Tregs regulate the immune response to self and foreign antigens

and help prevent autoimmune diseases by maintaining immune homeostasis. In cancer, Tregs are involved in tumor development and progression by inhibiting effector cells and reducing anti-tumor immunity. In TNBC, infiltration of Tregs into the TIME is often associated with resistance to anti-PD-L1 therapy and poor patient survival. Therefore, a better understanding of the mechanisms regulating the numbers of Tregs in the TIME of TNBC is necessary to tackle the problem of immunotherapy resistance. Claudin-low breast tumors are known to have increased numbers of tumor-infiltrating lymphocytes, specifically Tregs, as well as upregulated expression levels of ADAM12, an active ADAM metalloprotease. My goal was to investigate the role of ADAM12 in T cell accumulation to the tumor microenvironment *in vivo* using a mouse transplantation model of claudin-low breast cancer. Specifically, I investigated the accumulation of Tregs and other T cell subsets to tumors with or without expression of ADAM12. I found that the frequency of Tregs in tumor immune infiltrates was increased in tumors that lacked ADAM12 expression. Collectively, these findings give insight into the complex regulatory roles that PD-L1 and Tregs play in the breast cancer TIME.

Table of Contents

List of Figures viii

List of Tables ix

List of Abbreviations x

Acknowledgements xii

Dedication xiii

Chapter 1 - Literature Review 1

Triple Negative Breast Cancer 1

The Claudin-Low Subtype 1

The Tumor Immune Microenvironment 3

Regulators of the Tumor Immune Microenvironment 4

PD-1 5

PD-L1 6

Regulatory T Cells 6

Cancer Immunotherapy 7

Difficulties with Immune Checkpoint Blockade in Triple Negative Breast Cancer 8

Matrix Metalloproteases 9

ADAMs 9

ADAM10 10

ADAM17 10

ADAM12 10

Main Goals of Study 12

Chapter 2 - Proteolytic Processing of PD-L1 by ADAM Proteases in Breast Cancer Cells 13

Abstract 14
Introduction 15
Materials and Methods 17
Reagents and Antibodies 17
Cell Culture 17
Stable Overexpression of PD-L1 18
PD-L1 ELISA 19
Immunblotting 19
Results 20
Discussion 27
Chapter 3 - Role of ADAM12 in T Cell Accumulation in the Tumor Microenvironment 46
Abstract 47
Introduction 48
Materials and Methods 50
Antibodies and Reagents 50
Cell Culture 51
Concanavalin A Sepharose Purification of ADAM12 51
Establishment of ADAM12 Knockout in T11 Mouse Breast Cancer Cell Line 51
Immunoblotting 52
Mice Injections 52
Isolation of Tumor Infiltrating Lymphocytes 53
Flow Cytometry 54
Results 56

Discussion 59

Chapter 4 - Conclusions 75

References 78

Appendix A - Copyright Permissions 89

List of Figures

Figure 2.1 Interferon-γ increases PD-L1 protein levels in cell lysates and in culture media. 32

Figure 2.2 Elevated levels of soluble PD-L1 in culture media after stable overexpression of transmembrane PD-L1. 33

Figure 2.3 Soluble PD-L1 is generated by a proteolytic cleavage of transmembrane PD-L1..... 34

Figure 2.4 Detection of the C-terminal proteolytic fragment of PD-L1. 36

Figure 2.5 Cleavage of transmembrane PD-L1 is mediated by ADAM10 and ADAM17. 37

Figure 2.6 The effect of ADAM10 and ADAM17 knockdown on the cleavage of PD-L1. 40

Figure 3.1 Verification of donor integration during CRISPR/Cas9 by flow cytometry 62

Figure 3.2 Verification of ADAM12 KO in T11 cells by Western blotting 63

Figure 3.3 *In vitro* cell growth curve of wild-type and ADAM12 KO T11 cells 64

Figure 3.4 *In vivo* growth curves for wild-type and ADAM12 KO tumors 65

Figure 3.5 Absolute count of leukocytes per gram of T11 tumor 66

Figure 3.6 Percent of T cells, NK cells and dendritic cells among tumor-infiltrating leukocytes 67

Figure 3.7 Percent of helper T cells, cytotoxic T cells, natural killer T cells and γδ T cells among CD3+ cells 68

Figure 3.8 Percent of regulatory T cells among CD4+ T cells, all T cells, and all leukocytes. ... 70

List of Tables

Table 3.1 Antibodies and Reagents 50

List of Abbreviations

ADAM	A disintegrin and metalloprotease
AEBSF	4-(2-Aminoethyl) benzenesulfonyl fluoride hydrochloride
APP	Amyloid precursor protein
BCA	Bicinchoninic acid
BFP	Blue fluorescent protein
COSMIC	The catalogue of somatic mutations in cancer database
CTL	Cytotoxic T lymphocyte
CTLA-4	Cytotoxic T lymphocyte associated protein 4
DMEM	Dulbecco's modified Eagle's medium
DPBS	Dulbecco's phosphate buffered saline
ECM	Extracellular matrix
EGFR	Epidermal growth factor receptor
ER	Estrogen receptor
FcγRIII	Low-affinity immunoglobulin gamma Fc region receptor III
FDA	Food and drug administration
GAPDH	Glyceraldehyde 3-phosphate dehydrogenase
GEO	Gene expression omnibus
HER2	Human epidermal growth factor receptor 2
HOPS	Homotypic fusion and vacuole protein sorting
HS	Horse serum
ICOS	Inducible T cell costimulator
KO	Knockout

LAG-3	Lymphocyte activation gene 3 protein
M/F	Myc/FLAG tag
MMP	Matrix metalloprotease
NKT	Natural killer T cell
PD-1	Programmed cell death protein 1
PD-L1	Programmed death ligand 1
PMA	Phorbol 12-myristate 13-acetate
PR	Progesterone receptor
siRNA	Small interfering RNA
sPD-L1	Soluble programmed death ligand 1
TAPI-2	Tumor necrosis factor protease inhibitor 2
TGF	Transforming growth factor
TIME	Tumor immune microenvironment
TLS	Tertiary lymphoid structures
TNBC	Triple negative breast cancer
TNF	Tumor necrosis factor
Tregs	Regulatory T cells
VPS18	Vacuolar protein sorting-associated protein 18

Acknowledgements

First and foremost, I would like to express my deepest gratitude to my advisor Dr. Anna Zolkiewska, who guided me through my graduate education. I am extremely thankful for her constant support, patience and useful advice during the last two years. Her passion and expertise in the field inspired my motivation and love of this research field. I would not be the scientist I am today without her mentorship.

I would also like to express my deepest appreciation to my committee members Dr. Maureen Gorman and Dr. Sherry Fleming for their advice and helpful feedback.

I would like to thank all my colleagues in the Department of Biochemistry at Kansas State University. In particular, I would like to thank Dr. Indhujah Thevarajan and Guanpeng Wang for their insight, feedback and support in this project. I have truly enjoyed their friendship.

Additionally, I would like to thank my family, both the Romeros and the Fisers for their love and encouragement. Finally, I would like to thank my husband, Chad Fiser. I would not have been able to do this without his unconditional love, support and encouragement.

Dedication

I dedicate this work to my parents, Maribel Romero and Juan Carlos Vasquez, whose support and love made this all possible.

Chapter 1 - Literature Review

Triple Negative Breast Cancer

Breast cancer is one of the most common cancers worldwide and is a leading cause of cancer death in women. Although many factors contribute to the stratification of breast cancer subtypes, characterization based on receptor status has proven to be the most useful in predicting patient prognosis and responsiveness to treatment [1]. The expression of an estrogen receptor (ER), progesterone receptor (PR) and overexpression of human epidermal growth factor receptor 2 (HER2) is measured by immunohistochemical techniques and breast cancer subtypes are then classified by the presence or absence of these receptors. Triple negative breast cancer (TNBC) is defined by the lack of expression of an estrogen receptor, progesterone receptor and human epidermal growth factor receptor-2 [2], [3]. TNBC tumors are aggressive, highly invasive and show a relatively low response to therapeutics. TNBC represents only 15-20% of breast cancer, however, recurrence and mortality in this subtype is significantly worse than in other subtypes [2]. Treatment of TNBC is particularly challenging because this subtype does not respond well to targeted therapies and as such is treated with conventional methods including chemotherapy, often leading to systemic relapse. Considering the poor prognosis of TNBC and the high death rate of metastatic breast cancer, more research is needed to improve the clinical outcome of this subtype of breast cancer.

The Claudin-Low Subtype

Precise molecular stratification of breast cancer subtypes has become increasingly important in the current generation of anticancer treatments based on biological mechanisms. In the last two decades, genomic studies have established five breast cancer molecular subtypes: Luminal A, Luminal B, HER2-enriched, Claudin-low and Basal-like [4]–[6]. Luminal A and B

subtypes are distinguished by their expression of proliferation/cell cycle-related genes and luminal/hormone-related genes, with luminal B tumors having higher expression of proliferation/cell cycle genes and lower expression of luminal genes when compared to luminal A tumors [5]. The HER2-enriched subtype is characterized by high expression of HER2 and proliferation-related genes, intermediate expression of luminal genes and low expression of basal-related genes [5]. The basal-like subtype is characterized by high expression of proliferation genes and keratins normally expressed by the basal layer of the skin, intermediate expression of HER2 genes and very low expression of luminal genes [5].

The Claudin-low subtype is characterized by its low expression of genes involved in tight-junctions and cell-cell adhesion, including claudin-3, claudin-4, claudin-7, occludin and E-cadherin [6]. This subtype is triple negative and represents 25-40% of all TNBC. Gene clustering analysis of human breast tumors has shown that the claudin-low subtype clusters next to the basal-like subtype, due to their shared relatively low expression of Her2 and luminal genes [6]. Claudin-low tumors also have increased expression of genes involved in epithelial-to-mesenchymal transition [1], [6]. Furthermore, claudin-low tumors have been shown to have high expression of immune system response genes which are known to be expressed by T- and B-lymphocytes, suggesting high immune cell infiltration in this tumor subtype [6], [7]. Overall, claudin-low breast cancer is associated with poorer prognosis as well as decreased sensitivity to chemotherapy when compared to other subtypes [1], [6], [7]. Phenotypic characteristics of this subtype include high tumor grade, large tumor size, extensive lymphocytic infiltration and circumscribed tumor margins [7].

The Tumor Immune Microenvironment

The tumor immune microenvironment (TIME) refers to the immune cells, molecules and blood vessels that surround and interact with tumor cells. The TIME can consist of various types of cells including both innate and adaptive immune cells. For the purpose of this dissertation, I have focused on adaptive immune cells present in the TIME. T cells commonly identified by their expression of CD45 and CD3 cell surface markers are key players in the adaptive immune response. The main types of T cells are CD4+ and CD8+ T cells. CD8+ T cells are cytotoxic T cells, which are known for recognizing cells expressing tumor specific antigens and killing them via perforin- or granzyme-mediated mechanisms [8], [9]. CD4+ T cells include helper T cells and regulatory T cells (Tregs). Helper T cells are known for releasing a variety of cytokines regulating other immune cells. Tregs, identified by expression of the transcription factor FoxpP3 and cell surface marker CD25, suppress antitumor immune responses in the TIME [8]. Other types of T cells present in the TIME include gamma delta (γδ) T cells and natural killer T (NKT) cells.

Analysis of patients treated with immunotherapies has shown that there are certain classes of TIMEs that are associated with tumors prone to immunotherapy responsiveness, specifically to immune checkpoint blockade. Specifically, TIME responsiveness to immunotherapy is heavily influenced by the composition, function and location of immune cells within the TIME, as well as the interactions of immune cells with tumor cells. In general, TIMEs are classified according to broad criteria, which focus on the composition of immune cell infiltrates and the character of the inflammatory response [10]. There are currently three broad classes of TIMEs: infiltrated-excluded TIME, infiltrated-inflamed TIME and infiltrated-tertiary lymphoid structures (TLS) TIME [10]. Infiltrated-excluded TIME is broadly populated with

immune cells but is mostly void of cytotoxic T lymphocytes (CTLs) in the tumor core with high CTL presence along the tumor periphery. CTLs in this TIME are localized around the border of the tumor, in the invasive margin, where they can be found in contact with immunosuppressive tumor-associated macrophages or "stuck" in fibrotic nests. This TIME is considered poorly immunogenic due to low expression of the activation markers *GZMB* and *IFNG*, indicating an immunologically "cold" environment [10]. Infiltrated-inflamed TIME has high infiltration of leukocytes and CTLs, specifically those expressing PD-1, as well as PD-L1 expressing tumor cells [10] (see below for the description of PD-1 and PD-L1). This TIME is considered highly immunogenic due to the presence of highly activated CTLs in the tumor core. Infiltrated-TLS TIME is a subclass of infiltrated-inflamed environment, which displays histological evidence of tertiary lymphoid structures. These structures are lymphoid aggregates with similar cellular composition to the lymph nodes, including B cells, dendritic cells and Treg cells [10]. This TIME is thought to be immunogenic and is often correlated with a positive prognosis. Further analysis of the TIME could reveal biomarkers that could identify patient populations responsive to immunotherapies. Currently, there is a need to further characterize the TIME, specifically by identifying unifying features and critical differences that define distinct subclasses of the TIME and relating them to the likelihood of response to immunotherapy.

Regulators of the Tumor Immune Microenvironment

Some cell types present in the tumor microenvironment are responsible for the immunosuppressive environment and tumor immune escape, deeming these cell types potential targets for cancer immunotherapy. In general, the so called "regulators" of the tumor immune microenvironment include lymphoid cells, specifically regulatory T cells (Tregs), and immune checkpoint proteins like PD-1 and PD-L1. Within the tumor immune microenvironment, Tregs

play important regulatory roles by promoting tumor progression and modulating the function of tumor-infiltrating lymphocytes. Like Tregs, immune checkpoint proteins are also involved in dulling T cell activation and function. Other T cell subsets including cytotoxic T cells, gamma delta T cells, helper T cells and natural killer T cells also play important regulatory roles by promoting the surveillance and ultimate killing of tumor cells.

PD-1

Programmed cell death protein 1 (PD-1) is a 55-kDa type I transmembrane glycoprotein containing 288 amino acids [11], [12]. It has an extracellular IgV-like N-terminal domain, a membrane-permeating domain and a cytoplasmic tail [12]. The extracellular domain shares a 15-33% amino acid sequence identity with CD28 and ICOS, two co-stimulatory molecules and CTLA-4, a negative regulator of T cell responses [11], [12]. PD-1 is expressed on the surface of T cells, B cells, natural killer T cells, monocytes, macrophages and dendritic cells. Most importantly, PD-1 is highly expressed on tumor-specific T cells [12]. A key physiological function of PD-1 is the negative regulation of immune responses and maintaining peripheral self-tolerance. Therefore, PD-1 is an important inhibitory immune checkpoint protein.

Although the physiological roles of PD-1 are beneficial, PD-1 can also be harmful in the context of cancer. In cancer, PD-1 expression is a major immune escape mechanism. Tumor cells exploit this mechanism by expressing the PD-1 ligands, therefore evoking a “shield” that allows them to evade immune surveillance and T cell mediated killing. PD-1 binds to one of the two ligands, PD-L1 or PD-L2 [12], [13]. Contrary to its name, PD-1 does not directly induce cell death but instead has been shown to reduce survival signals necessary for cell proliferation. Interaction of PD-1 with PD-L1 or PD-L2 induces downregulation of T cell activity, reduces

cytokine production, induces T cell lysis and causes tolerance to antigens. PD-1 blockade and inhibition has become a promising therapeutic approach in treating various types of cancers.

PD-L1

Programmed Cell Death Ligand 1 (PD-L1) is a 33-kDa type 1 transmembrane glycoprotein that contains IgV and IgC domains in its extracellular region [12]. PD-L1 is usually expressed by macrophages, activated T cells and B cells, dendritic cells and some epithelial cells [12]. Most importantly, PD-L1 is also expressed by tumor cells. It's expression on tumor cells is a mechanism to escape antitumor responses mounted by adaptive immunity. Specifically, PD-L1 expression is implicated in tumor progression. PD-L1 is involved in the dulling of T cell immune responses and, when bound to PD-1, it reduces the proliferation of PD-1 positive cells by inhibiting their cytokine secretion and inducing apoptosis. Expression of PD-L1 in breast cancer has been associated with large tumor size, high grade, high proliferation, estrogen receptor-negative status, and is inversely correlated with patient survival [13]. Interestingly, 20% of triple negative breast cancers express PD-L1, making it an important target for immune checkpoint blockade.

Regulatory T Cells

Regulatory T cells (Tregs) are defined as a T cell population that can modulate the immune system, maintain self-tolerance and prevent autoimmune disease [14]. Specifically, Tregs are thought to be responsible for inducing and maintaining peripheral tolerance. Functionally mature Tregs are produced in the thymus but can also be induced from naïve T cells in the periphery. Tregs are characterized as CD4+CD25+FOXP3+ T cells, with FOXP3 being the master regulator of Treg cells [15].

Tregs are immunosuppressive cells whose suppression mechanisms can be grouped into four basic modes of action: 1) production of inhibitory cytokines, 2) cytolysis, 3) metabolic disruption and 4) modulation of dendritic cell maturation or function [15]. There are three main inhibitory cytokines, IL-10, IL-35 and TGF-beta, which are key mediators of Treg function. Furthermore, activated human natural Tregs have been shown to express granzyme B, a serine protease which facilitates granule-mediated apoptosis of natural killer cells and CTLs [15]. Lastly, Tregs have been shown to negatively modulate the maturation and/or function of dendritic cells that are required for effector T-cell activation [15].

Cancer Immunotherapy

Cancer immunotherapy is a relatively new option for cancer treatment that can be used in conjunction with traditional treatments including chemotherapy, radiation and surgery [16]. Cancer immunotherapy is a type of treatment that takes advantage of a person's own immune system to help kill cancer cells. Currently, there exists many different types of immunotherapies designed to target tumor cells and work with the immune system at different levels. Some of these anticancer immunotherapies include targeted antibodies, cancer vaccines, adoptive cell therapy, immunomodulators including immune checkpoint blockade and oncolytic virus therapy [16], [17].

Cancer immunotherapies targeting immune checkpoint proteins, specifically immune regulators, have recently revolutionized cancer treatments. Immune checkpoint blockade therapies, work by manipulating the "brakes" and "gas pedals" of the immune system [17]. Specifically, these treatments block the receptor and/or ligand interactions of molecules such as cytotoxic T-lymphocyte associated protein 4 (CTLA-4), PD-L1 and PD-1, that are involved in dulling T cell activation or function [18]. CTLA-4 is a co-inhibitory protein expressed on the

surface of cancer cells, Tregs and sometimes upregulated in other types of T cells [16], [18]. CTLA-4 blockade therapy prevents its interaction with its ligands, CD80 and CD86 expressed on antigen presenting cells, which leads to up-regulation of T cell activity [16], [19]. In 2011, the US Food and Drug Administration (FDA) approved anti-CTLA-4 antibodies (ipilimumab) as a therapy for the treatment of advanced melanoma. PD-1 binding to PD-L1 promotes the dephosphorylation of T cell receptor signal components and leads to the inhibition of signaling pathways, thereby decreasing T cell proliferation, survival, cytokine production and other effector functions [16]. Thus, PD-1/PD-L1 blockade therapy restores antitumor immune responses and promotes immune-mediated elimination of tumor cells. Currently, there are several FDA-approved checkpoint blockade therapies for this interaction, including anti-PD-1 antibodies (nivolumab, pembrolizumab and cemiplimab) and anti-PD-L1 antibodies (atezolizumab, avelumab and durvalumab), which treat several different types of human cancers [16].

Difficulties with Immune Checkpoint Blockade in Triple Negative Breast Cancer

Although advances in immune checkpoint blockade therapies have been vast, these therapies have only shown significant clinical benefits for a minority of patients. Specifically, response rates to PD-1/PD-L1 blockade range between 20-38% among various tumor types, indicating that there is an unmet clinical benefit for the majority of patients who do not respond to checkpoint blockade therapies [10], [16]. Recently, analysis of patient populations treated with immune checkpoint blockade has revealed that response variability may be due to the relationship between tumor and immune cells. Additionally, tumor-infiltrating lymphocytes may contribute to tumor progression through immune suppression or the production of cytokines that regulate cell proliferation, migration and angiogenesis [18], [20]. In breast cancer, specifically in

the claudin-low subtype, there is an increased expression of immune genes and greater numbers of tumor-infiltrating lymphocytes, with a focal increase in Tregs [18], [20]. This suggests that increased expression of Tregs may be a possible mechanism by which immune infiltration is associated with a poor prognosis and low immune checkpoint blockade response rates in claudin-low tumors [20]. Overall, a better understanding of the interactions between tumor-infiltrating lymphocytes and immunotherapy is essential to improve the efficacy of immune checkpoint blockade therapies.

Matrix Metalloproteases

Matrix Metalloproteases (MMPs) are the family of 24 human zinc-binding endopeptidases that can degrade extracellular matrix components [21], [22]. The main function of MMPs is the degradation of extracellular matrix molecules but they have also been shown to play key roles in morphogenesis, wound healing, tissue repair, remodeling in response to injury and in the progression of diseases such as cancer [22]. MMP structure consists of a pro-peptide, a catalytic metalloprotease domain, a linker peptide and a hemopexin domain. A zinc binding motif, HEXXHXXGXXH, in the catalytic domain and a “cysteine switch” motif, PRCGXPD, in the pro-peptide are common structural signatures of MMPs [22].

ADAMs

A Disintegrin And Metalloproteases (ADAMs) are members of the same zinc protease superfamily that includes MMPs. The domain structure of ADAMs consists of a prodomain, a metalloprotease domain, a disintegrin domain, a cysteine-rich domain, an EGF-like domain, a transmembrane domain and a cytoplasmic tail [23]. Thus, ADAMs are membrane anchored proteases that have the catalytic domain similar to MMPs but lack a hemopexin-like domain [21]. ADAMs have been implicated in various biological activities including cytokine and

growth factor shedding, cell migration and other processes including muscle development or inflammation [23]. Interestingly, recent findings have suggested roles for ADAMs in various human diseases including breast cancer [21], [23], [24].

ADAM10

Considered one of the best characterized sheddases, a protease which cleaves a membrane protein substrate close to or within its transmembrane domain [25], ADAM10 is known to be mostly active in the trans-Golgi network, the late secretory pathway compartments, and at the plasma membrane [25]. Currently, over 100 substrates in different tissues have been identified for ADAM10, which are known to be involved in many biological processes. Most notably, ADAM10 mediates ligand-dependent cleavage of the Notch receptor, which regulates Notch signaling required for embryonic development. ADAM10 also acts as an alpha-secretase for the amyloid precursor protein (APP).

ADAM17

ADAM17 is another well characterized sheddase, and its activity is mostly observed when cells are stimulated with either physiological activators or phorbol esters such as PMA. ADAM17 plays a key function in tissue homeostasis through its cleavage of various members of the epidermal growth factor receptor ligand family, specifically TGF alpha [25]. ADAM17 is also considered a major drug target for inflammatory diseases due to its role as a major protease for the cytokine tumor necrosis factor (TNF) alpha [24], [25]. Recently, ADAM17 has been shown to play a role in the development and progression of multiple cancers due to its implication in cancer initiation, progression and its role in conferring resistance to specific cancer therapies [24], [26].

ADAM12

ADAM12 is an active metalloprotease involved in cell adhesion, extracellular matrix restructuring and cell signaling [27]. In humans, ADAM12 exists in two forms: a transmembrane form, ADAM12-L, and an alternatively spliced secreted form, ADAM12-S [27]. It is expressed at low levels in cartilage, bone, muscle, adipose tissue, liver, uterus and brain [27], [28]. Specifically, ADAM12-L is expressed at low levels in normal epithelial cells, but significantly higher levels of ADAM12-L are present in various human carcinomas, including small cell lung cancer and breast cancer [27], [29], [30]. Proteolytic substrates of ADAM12 include Delta-like 1 [31], a mammalian Notch receptor ligand, and epidermal growth factor receptor (EGFR) ligands [29]. The *ADAM12* gene expression is regulated both at the transcriptional and post-transcriptional levels. Most notably, *ADAM12* expression is upregulated by transforming growth factor beta 1 [32] and Notch signals [33], and is down-regulated post-transcriptionally by microRNA-29 and microRNA-200 [34], [35].

Importantly, many ADAM species including ADAM10, ADAM17 and ADAM12 have been implicated in cancer cell proliferation and progression, making them important biomarkers and therapeutic targets. Specifically, ADAM12 has been shown to be upregulated in TNBC, including the claudin-low molecular subtype [29], [36]. Interestingly, ADAM12 was found to contribute to the cancer stem cell-like phenotype of claudin-low breast tumors [29]. This is important because breast cancer stem cells are mostly responsible for tumor maintenance, treatment resistance and disease recurrence [29]. ADAM12 has also been reported to cleave several ECM molecules, including gelatin, type IV collagen and fibronectin [26], suggesting a possible role in priming the primary tumor niche for cancer cell invasion and tumor metastasis. Furthermore, ADAM12 was found to accelerate tumor progression in a mouse breast cancer model by decreasing tumor cell apoptosis while simultaneously increasing stromal cell apoptosis

[37]. Overall, ADAM12 seems to play an essential role in the progression of triple negative breast cancer.

Main Goals of Study

Although TNBCs represent only a small percent of all breast cancers, their aggressiveness, higher mortality rate and, most importantly, their low response to therapeutics render this subtype an important research target. Clearly, a better insight into the biological interactions in the tumor immune microenvironment is needed. In this dissertation, I aimed to study the various regulators of the tumor immune microenvironment in TNBC and gain insight into their influence on cancer progression.

- One goal was to investigate the cleavage of PD-L1, a known suppressor of anti-tumor immunity, expressed on the surface of tumor cells.
    - I was able to show that cleavage of PD-L1 is mediated by ADAM10 and ADAM17, two members of the ADAM family of ADAM metalloproteases.
- Studies have shown that ADAM12 is upregulated in claudin-low breast cancer, which is characterized by high immune cell infiltration [7], [37], [38]. My goal was to explore the role of ADAM12 in T cell accumulation to the tumor microenvironment *in vivo*. I investigated the accumulation of regulatory T cells, cytotoxic T cells, gamma delta T cells, helper T cells and natural killer T cells to the tumor microenvironment in claudin-low breast tumors with or without expression of ADAM12.
    - I looked at non-cell autonomous effects of ADAM12 knockout in the tumor immune microenvironment. I showed that the percent of regulatory T cells is increased in claudin-low breast tumors lacking ADAM12.

Chapter 2 - Proteolytic Processing of PD-L1 by ADAM Proteases in Breast Cancer Cells

Reprinted by permission from [Springer Nature Customer Service Centre GmbH]: [Springer Nature] [Cancer Immunology, Immunotherapy] [Romero, Y., Wise, R. & Zolkiewska, A. "Proteolytic Processing of PD-L1 by ADAM Proteases in Breast Cancer Cells." Cancer Immunology, Immunotherapy: CII vol. 69,1 (2020): 43-55. https://doi.org/10.1007/s00262-019-02437-2]

Abstract

Expression of programmed death ligand 1 (PD-L1) on the surface of tumor cells and its interaction with programmed cell death protein 1 (PD-1) on tumor-infiltrating lymphocytes suppress anti-tumor immunity. In breast tumors, PD-L1 expression levels are the highest in estrogen receptor-negative, progesterone receptor-negative, and human epidermal growth factor receptor 2-negative (triple-negative) cancers. In this study, we show that a portion of PD-L1 exogenously expressed in several triple-negative breast cancer cell lines, as well as endogenous PD-L1, is proteolytically cleaved by cell surface metalloproteases. The cleavage generates an ~ 37-kDa N-terminal PD-L1 fragment that is released to the media and a C-terminal PD-L1 fragment that remains associated with cells but is efficiently eliminated by lysosomal degradation. We identify ADAM10 and ADAM17, two closely related members of the ADAM family of cell surface metalloproteases, as enzymes mediating PD-L1 cleavage. Notably, treatment of cells with ionomycin, a calcium ionophore and a known activator of ADAM10, or with phorbol 12-myristate 13-acetate, an activator of ADAM17, dramatically increases the release of soluble PD-L1 to the media. We postulate that ADAM10 and/or ADAM17 may contribute to the regulation of the PD-L1/PD-1 pathway and, ultimately, to anti-tumor immunity in triple-negative breast cancer.

Introduction

Immune checkpoint blockade represents one of the most promising immunotherapies for the treatment of solid tumors. The therapy involves blocking the interaction between a negative immune checkpoint regulator, such as programmed cell death protein 1 (PD-1) on T cells, with programmed death ligand 1 (PD-L1) expressed in the tumor microenvironment [39]. Since the PD-1/PD-L1 pathway attenuates T cell activity and promotes tumor immune escape, anti-PD-1/PD-L1 therapeutics can stimulate anti-tumor responses, reduce tumor growth, or even cause tumor remission in patients with advanced cancers [39]. In breast cancer, the PD-1/PD-L1 axis is considered a particularly promising therapeutic target in triple-negative tumors (estrogen receptor-negative, progesterone receptor negative, human epidermal growth factor receptor 2-negative) [40]. Triple-negative breast cancer (TNBC) is the most immunogenic breast cancer subtype, with more prominent immune infiltration and higher expression levels of PD-L1 than other tumor subtypes [41], [42]. Within tumors, PD-L1 is expressed both in tumor cells and in tumor-infiltrating lymphocytes, including CD4+ or CD8+ T cells, and macrophages [41], [42]. Despite the favorable immune characteristics of TNBCs, their response to anti-PD-1/PD-L1 therapy is rather modest and varies significantly among patients [40]. Recently reported objective response rates to anti-PD-1/PD-L1 monotherapies in patients with metastatic TNBCs remained below 25% [43], [44], and response rates to a combination of anti-PD-L1 antibody plus chemotherapy were lower than 60% [45]. To further improve therapeutic outcomes of PD-1/PD-L1 blockade and to help identify biomarkers that can predict patient's response to anti-PD-1/PD-L1 therapies, a better understanding of all aspects of the PD-1/PD-L1 pathway is needed, including the role of tumor-derived PD-L1 and its regulation in tumor cells. PD-L1 gene expression is regulated at the transcriptional and post-transcriptional levels [46], and PD-L1

protein is further regulated post-translationally via ubiquitination, glycosylation, palmitoylation, or lysosomal degradation [47]–[51]. Transmembrane PD-L1, the main protein isoform of PD-L1, resides at the cell surface, but also on the surface of exosomes that are secreted to the extracellular milieu [52], [53]. Soluble forms of PD-L1, containing an intact receptor binding domain and lacking the transmembrane domain, have also been described, and they result either from an alternative PD-L1 mRNA splicing [54], [55] or from cleavage of the transmembrane PD-L1 protein. Proteolytic cleavage of PD-L1 was described in renal cell carcinoma [56], mesenchymal stromal cells [57], [58], and head and neck squamous cell carcinoma [59], but it has not been investigated in breast cancer. In this study, we demonstrate unambiguously a proteolytic cleavage of PD-L1 in triple-negative breast cancer cell lines. The cleavage generates a distinct soluble N-terminal PD-L1 fragment, which is detectable by ELISA and immunoblotting, and a C-terminal PD-L1 fragment that remains associated with cells but is efficiently eliminated by lysosomal degradation. We also identify a disintegrin and metalloprotease 10 (ADAM10) and ADAM17, two closely related members of the ADAM family of cell surface metalloproteases [60], as enzymes mediating PD-L1 cleavage. We postulate that ADAM10 and/or ADAM17 may contribute to the regulation of the PD-L1/PD-1 pathway and, ultimately, to anti-tumor immunity in TNBC.

Materials and Methods

Reagents and Antibodies

Recombinant human IFN-γ was from eBioscience (San Diego, CA), batimastat, aprotinin, pepstatin, leupeptin, matrix metalloprotease (MMP)-9 inhibitor I, GI254023X, CL-82198, bafilomycin A1, monensin, ammonium chloride, and phorbol 12-myristate 13-acetate (PMA) were from MilliporeSigma (Burlington, MA), AEBSF was from Fisher Scientific (Hampton, NH), ionomycin and tumor necrosis factor protease inhibitor 2 (TAPI-2) were from Cayman Chemical (Ann Arbor, MI). Fetal bovine serum (FBS) and horse serum (HS) were from Gibco Thermo Fisher Scientific (Waltham, MA). ON-TARGETplus human ADAM10 small interfering RNAs (siRNAs; J-004503-06 and J-00450307; siA10#1 and siA10#2, respectively), siGENOME human ADAM17 siRNAs (D-003453-02 and D-00345303; siA17#1 and siA17#2, respectively), and Dharmafect 4 transfection reagent were from Dharmacon (Lafayette, CO). Human PD-L1 DuoSet ELISA kit was from R&D Systems (Minneapolis, MN). Anti-PD-L1 mAbs, clones E1L3N and E1J2J, anti-ADAM10 pAb #14194, and anti-glyceraldehyde 3-phosphate dehydrogenase (GAPDH) mAb, clone D16H11, were from Cell Signaling Technology (Danvers, MA), anti-ADAM17 pAb was from QED Bioscience (San Diego, CA), anti-Myc tag mAb, clone 9E10, was from Invitrogen (Carlsbad, CA), and anti-FLAG tag mAb (DYKDDDDK) was from GenScript (Piscataway, NJ).

Cell Culture

MDA-MB-231, BT549, MCF10A, A549, and DU-145 cells were from the American Tissue Culture Collection (Manassas, VA). SUM149 and SUM159 cell lines were obtained from Asterand (Detroit, MI). MDA-MB-231, DU-145, and A549 cells were cultured in DMEM/F12 medium with 10% FBS and 10 mM HEPES. BT549 cells were grown in RMPI-1640 medium

containing 10% FBS and 5 μg/ml insulin. SUM149 and SUM159 cells were cultured in Ham's F-12 medium supplemented with 5% FBS, 10 mM HEPES, 5 μg/ml insulin, and 1 μg/ml hydrocortisone. MCF10A cells were cultured in DMEM/F-12 supplemented with 5% horse serum, 0.5 μg/ml hydrocortisone, 20 ng/ml human EGF, and 10 μg/ml insulin. Cells were maintained at 37 °C under humidified atmosphere containing 5% CO_2. siRNA transfections were performed using 50 nM siRNA (total concentration) and 2 μl Dharmafect 4 (for MDA-MB-231 cells) or Dharmafect 2 reagent (for A549 and DU-145 cells) per well in six-well plates. One day after transfection, cells were transferred to fresh complete media and incubated for additional 24–48 h.

Stable Overexpression of PD-L1

Cells were plated in 12-well plates ($1x10^5$ cells/well). The next day, 2 ml of fresh media containing human PD-L1 (NM_014143) lentiviral particles ($2x10^5$ transducing units/ well; OriGene, Rockville, MD) and polybrene (8 μg/ml) were added. Two different PD-L1 clones were used: Myc/ FLAG (M/F)-tagged (RC213071L3V) and GFP-tagged (RC213071L4V). The M/F-tagged construct contained the following C-terminal sequence after the PD-L1 insert: TRTRPLEQKLISEEDLAANDILDYKDDDDKVWV*GSGATNFSLLKQAGDVEENP*, with the Myc and FLAG tags underlined and the P2A peptide sequence italicized. The GFP-tagged construct also contained the C-terminal P2A sequence. P2A is a self-cleaving peptide that separated PD-L1-M/F or PD-L1-GFP and puromycin N-acetyl transferase encoded in the expression vectors. In parallel, cells were incubated with control GFP lentiviral particles (PS100093V). After 24 h, cells were transferred to fresh media, re-plated into six-well plates, and incubated with puromycin for the next 7–10 days. The optimal concentrations of puromycin for each cell line were determined by performing kill curve experiments and were as follows:

MDA-MB-231, 0.4 μg/ml; BT549, 0.3 μg/ml; MCF10A, 1 μg/ml; SUM159, 1 μg/ml; SUM149, 0.3 μg/ml; A549, 0.5 μg/ml; and DU-145, 0.5 μg/ml.

PD-L1 ELISA

Cells were incubated in six-well plates for 24–72 h in media with various treatments, as indicated. Conditioned media were centrifuged for 15 min at 21,000×g, and concentrations of soluble PD-L1 (sPD-L1) in the supernatants were measured using human PD-L1 DuoSet ELISA kit (R&D Systems) and a BioTek H1M microplate reader. Cells remaining attached to plates were lysed with lysis buffer, and protein concentrations were determined using the bicinchoninic acid (BCA) assay (Thermo Fisher Scientific). To account for possible differences in cell densities between individual wells, sPD-L1 concentrations measured by ELISA were normalized to equal protein concentration in all cell lysates.

Immunblotting

Immunoblotting was performed, as described [29]. For signal detection, we used SuperSignal West Pico or West Femto chemiluminescence detection kit (Thermo Fisher Scientific) and Azure c500 digital imaging system.

Results

To determine whether PD-L1 is released from the surface of breast cancer cells, we measured concentrations of sPD-L1 in conditioned media from four different human TNBC cell lines, MDA-MB-231, BT549, SUM159, and SUM149, as well as from the untransformed human mammary cell line MCF10A, using a sandwich ELISA assay employing antibodies specific for the extracellular domain of PD-L1. In parallel, PD-L1 in cell lysates was examined by immunoblotting.

The amount of PD-L1 detected in the lysates of unstimulated cells was the highest in MDA-MB-231 cells and the lowest in SUM149 cells (MDA-MB-231>SUM159> BT549≈MCF10A>SUM149) (Figure 2.1 a). This order of expression corresponded well to PD-L1 mRNA levels determined by RNA sequencing [61], [62] (Gene Expression Omnibus (GEO): GSE73526 and GSE48213; https://www.ncbi.nlm.nih.gov/geo/). Concentrations of sPD-L1 in the conditioned media from unstimulated cells were very low, except for MDA-MB-231 cells, where sPD-L1 reached ~100 pg/ml (Figure 2.1 b). Stimulation of cells for 48 h with 10 ng/ml human IFN-γ dramatically increased cellular levels of PD-L1 (Figure 2.1 a), consistent with the known role of IFN-γ in the regulation of PD-L1 expression [63]. Importantly, treatment of cells with IFN-γ also significantly increased concentrations of sPD-L1 in the conditioned media from all five cell lines (Figure 2.1 b).

Human PD-L1 mRNA can be alternatively spliced, generating transcripts that are translated into soluble forms of PD-L1 protein [54], [55]. Similar to the main PD-L1 splice variant, these alternative variants are induced by IFN-γ [54]. To exclude the possibility that increased concentrations of sPD-L1 detected after stimulation with IFN-γ were simply due to an increased expression of a soluble PD-L1 isoform, we established cells with stable constitutive

overexpression of transmembrane PD-L1. Recombinant PD-L1 contained a C-terminal GFP tag or a tandem M/F tag. Immunoblotting of cellular lysates showed the presence of several PD-L1 bands, ranging from ~70 kDa to ~90 kDa for PD-L1-GFP, and from ~50-kDa to ~70-kDa for PD-L1-M/F (Figure 2.2 a), which was most likely due to post-translational protein modifications. Importantly, conditioned media from cells with stable overexpression of PD-L1 contained much higher concentrations of sPD-L1 than the parental cells, typically approaching 2-4 ng/ml for MDA-MB-231 cells, 0.4-1 ng/ml for the remaining breast cancer cells, and 0.2-0.75 ng/ml for MCF10A cells after a 2-day incubation period (Figure 2.2 b). After parallel measurement of PD-L1 concentrations in cell lysates by ELISA, we estimated that sPD-L1 released to the media represented ~5-10% of the total PD-L1 protein in breast cancer cells and ~1% of PD-L1 in MCF10A cells.

Next, we asked whether sPD-L1 represented an authentic cleavage product of transmembrane PD-L1. This question was important, because cancer cells often shed large amounts of exosomes [52], and PD-L1-containing exosomes might be detected by ELISA. We focused on three cell lines: MDA-MB-231-PD-L1-M/F, BT549-PD-L1-M/F, and MCF10A-PD-L1-M/F, with high, intermediate, and low secretion of sPD-L1, respectively. After centrifugation of the conditioned media at 120,000xg for 1.5 h, a standard method for sedimentation of exosomes [64], sPD-L1 was detected in the supernatants and not the pellets (Figure 2.3 a). This result indicated that PD-L1 detected in the conditioned media represented a soluble protein and not exosomal transmembrane PD-L1. Furthermore, incubation of cells in serum-free medium did not diminish the levels of sPD-L1 (Figure 2.3 b), indicating that cellular proteases, rather than proteolytic enzymes from the serum, played a role in generating sPD-L1.

To unambiguously demonstrate that sPD-L1 was generated by proteolytic cleavage of transmembrane PD-L1, we examined conditioned media from MDA-MB-231 cells overexpressing PD-L1 (which release the highest amounts of sPD-L1) by immunoblotting, using an antibody specific for the extracellular domain of PD-L1 (E1J2J). Cells were incubated in serum-free medium in this experiment to avoid interference from serum albumin in the detection of PD-L1. First, we observed low amounts of full-length PD-L1 in the conditioned media (Figure 2.3 c), which might be due to a slightly decreased cell viability in the absence of serum. Most importantly, we detected a ~37-kDa N-terminal PD-L1 fragment in conditioned media from MDA-MB-231 cells overexpressing PD-L1-M/F or PD-L1-GFP, but not in cell lysates (Figure 2.3 c). This fragment was not observed in conditioned media from control GFP cells, most likely because the level of endogenous sPD-L1 was below the antibody detection limit. Importantly, while the molecular weights of full-length PD-L1-M/F and PD-L1-GFP were different due to the presence of two different C-terminal tags, the size of the 37-kDa fragment released to the media was the same, indicating that this fragment must have been derived from the recombinant PD-L1-M/F and PD-L1-GFP proteins via the cleavage at the same site within the two constructs.

We next investigated the fate of the C-terminal fragment of PD-L1. If the 37-kDa N-terminal cleavage product is released to the media, a complementary C-terminal PD-L1 fragment should remain associated with cells. Inspection of the lower molecular weight region of the immunoblots obtained with the antibody specific for the cytoplasmic domain of PD-L1 (E1L3N) revealed the presence of a weak ~18-kDa band in the lysates of BT549 cells expressing PD-L1-M/F, but not in the lysates of control cells expressing GFP (Figure 2.4 a). To visualize the 18-kDa fragment in MDA-MB-231-PD-L1-M/F or MCF10A-PD-L1-M/F lysates, cells needed to be incubated for 24 h in the presence of 10 μM chloroquine, a weak base that leads to inhibition of

lysosomal protein degradation. Chloroquine treatment did not have a significant effect on full-length PD-L1-M/F (Figure 2.4 a). This result suggests that the 18-kDa cleavage product is not stable in MDA-MB-231 or MCF10A cells and is efficiently degraded by lysosomal enzymes. Chloroquine was not required for stabilization of the 18-kDa PD-L1 fragment in BT549 cells (Figure 2.4 a, see Discussion). The same 18-kDa band was also detected with anti-Myc and anti-FLAG antibodies (Figure 2.4 b), confirming that this band represented the C-terminal fragment of the PD-L1-M/F protein.

We next used three other drugs to inhibit lysosomal function: ammonium chloride, a weak base, monensin, a Na+/H+ ionophore, or bafilomycin A1, an inhibitor of vacuolar-type H+-ATPase (V-ATPase). As in the case of chloroquine, these treatments increase lysosomal pH and impair lysosomal protein degradation. In MDA-MB-231-PD-L1-M/F or MCF10A-PD-L1-M/F cells, an 18-h treatment with 10 mM NH4Cl or a 4-h treatment with 20 μM monensin or 0.1 μM bafilomycin A1 increased the abundance of the 18-kDa C-terminal PD-L1 fragment (Supplementary Figure 2.1,Supplementary Figure 2.2,Supplementary Figure 2.3). In BT549-PD-L1-M/F cells, these treatments did not have a major impact on the C-terminal PD-L1 fragment (Supplementary Figure 2.1,Supplementary Figure 2.2,Supplementary Figure 2.3), corroborating the results obtained with chloroquine.

Finally, we asked whether a similar C-terminal fragment can be detected after the cleavage of endogenous PD-L1. Parental MDA-MB-231, BT549, or MCF10A cells were incubated for 48 h with IFN-γ to boost PD-L1 expression, and for an additional 24 h with chloroquine to stabilize the putative C-terminal cleavage product. As shown in Figure 2.4 c, a weak 14-kDa band corresponding to the C-terminal PD-L1 fragment was detected in the lysates of IFN-γ- and chloroquine-treated MDA-MB-231 and MCF10A cells. The difference in the

molecular weight of this band and the C-terminal PD-L1-M/F fragment, 14 kDa versus 18 kDa, could at least partially be due to the presence of additional 53 residues in the PD-L1-M/F construct (predicted molecular weight of ~5.9 kDa, see Materials and Methods). Similar to BT549-PD-L1-M/F cells, in parental BT549 cells chloroquine did not have a major effect on the stability of the C-terminal PD-L1 fragment.

To determine which enzyme(s) mediate the cleavage of PD-L1, we first incubated cells with inhibitors of different classes of proteases. It was shown previously that high concentrations of ilomastat (GM6001), a broad-spectrum hydroxamate-based metalloprotease inhibitor, partially suppressed the release of sPD-L1 in mouse L-929 cells (connective tissue) [65]. Inhibitors of other classes of proteases have not been tested. Here, MDA-MB-231, BT549, or MCF10A cells overexpressing PD-L1-M/F were treated for 2 days with the following inhibitors: 5 μM batimastat, another broad-spectrum hydroxamate-based metalloprotease inhibitor, 0.1 mM AEBSF or 10 μg/ml aprotinin, two serine protease inhibitors, 10 μg/ml pepstatin, an aspartic protease inhibitor, or 10 μg/ml leupeptin, a cysteine protease inhibitor. In all three cell lines, the release of sPD-L1 was significantly decreased only by batimastat (Figure 2.5 a-c). These results indicated that PD-L1 cleavage was selectively mediated by member(s) of the metalloprotease family of enzymes.

Previous reports implicated two matrix metalloproteases, MMP-9 and MMP-13, in the cleavage of PD-L1 in human foreskin fibroblasts and in head and neck cancer cells [57], [59]. Our analysis of the results of global gene expression profiling of breast cancer cells by high throughput sequencing [61], [62] indicated, however, that the expression of MMP-9 and MMP-13 in MDA-MB-231, BT549, and MCF10A cells is very low (GEO:GSE73526 and GSE48213; https://www.ncbi.nlm.nih.gov/geo/). Since batimastat also inhibits ADAM metalloproteases, in

addition to MMPs, and since ADAM10 and ADAM17 are highly expressed in MDA-MB-231, BT549, and MCF10A cells, as well as in SUM159 and SUM149 cells [61], [62], we hypothesized that these two ADAMs may be involved in PD-L1 cleavage in our system. Indeed, treatment of MDA-MB-231, BT549, or MCF10A cells overexpressing PD-L1-M/F with 30 μM GI254023X, a known selective inhibitor of ADAM10 [66], or 30 μM TAPI-2, a selective inhibitor of ADAM17 [67], significantly decreased the release of sPD-L1 to the media (Figure 2.5 d-f). In contrast, incubation of cells with 1 μM MMP-9 Inhibitor I or 50 μM CL-82198, a specific MMP-13 inhibitor, did not block the release of sPD-L1 (Figure 2.5 d-f). Furthermore, the measured IC50 values for GI254023X (Figure 2.5 g) and TAPI-2 (Figure 2.5 h) in MDA-MB-231-PD-L1-M/F cells were 0.20 μM and 0.16 μM, respectively. These submicromolar IC50 values were similar to the IC50 values for GI254023X or TAPI-2 in ADAM10- or ADAM17-mediated cleavage reactions of model substrates in vitro [66], [67], suggesting that these ADAMs might be involved in the cleavage of PD-L1 in intact cells studied here.

To validate our results of pharmacological inhibition of ADAM10 and ADAM17, the two ADAMs were down-regulated using siRNAs. Transfection of two different siRNAs targeting ADAM10 into MDA-MB-231-PD-L1-M/F cells resulted in ~70% down-regulation of ADAM10 expression and ~60% inhibition of sPD-L1 release to the media (Figure 2.6 a, b). Transfection of two different siRNAs targeting ADAM17 led to almost complete loss of ADAM17 expression and 40-60% decrease of sPD-L1 in the media (Figure 2.6 a, b). Combination of all four siRNAs targeting both ADAM10 and ADAM17 resulted in ~80% inhibition of the release of sPD-L1 (Figure 2.6 b). Collectively, these results confirmed that the cleavage of transmembrane PD-L1-M/F in MDA-MB-231 cells was mediated, in a large part, by ADAM10 and ADAM17.

ADAM10 and ADAM17 expression is not restricted to breast cancer cells. To determine whether PD-L1 may be cleaved by ADAM10 and/or ADAM17 in other cancer cell types, we overexpressed PD-L1-M/F in DU-145 prostate cancer cells and A549 lung cancer cells (Supplementary Figure 2.4 a). In both cell lines, we detected increased levels of sPD-L1 in the conditioned media of PD-L1-M/F-expressing cells versus GFP-expressing cells (Supplementary Figure 2.4 b). ADAM10 or ADAM17 knockdown using siRNAs significantly decreased the concentration of sPD-L1 in the media (Supplementary Figure 2.4 c, d), indicating that ADAM10- and ADAM17-mediated cleavage of PD-L1-M/F is not restricted to breast cancer cells.

Notably, ADAM10 activity in cell-based assays can be rapidly up-regulated by the calcium ionophore ionomycin, whereas ADAM17 activity can be augmented after stimulation of protein kinase C with phorbol esters [68], [69]. Here, a 45-min incubation of MDA-MB-231-PD-L1-M/F cells with 1 µM or 2.5 µM ionomycin dramatically increased the release of sPD-L1. This effect was dose-dependent and was diminished in cells transfected with siRNAs targeting ADAM10 (Figure 2.6 c). Also, a 2-h treatment of cells with 25 ng/ml or 50 ng/ml PMA augmented the concentration of sPD-L1 in the media in a dose-dependent manner, and this effect was significantly reduced by transfection with siRNAs targeting ADAM17 (Figure 2.6 d). In sum, these results confirmed the role of ADAM10 and ADAM17 in PD-L1 cleavage and demonstrated that ADAM10- or ADAM17-mediated release of sPD-L1 from the cell surface can be rapidly and potently up-regulated by ionomycin-induced increase of intracellular concentrations of calcium ions or by stimulation of cells with PMA.

Discussion

Our studies provide evidence that human transmembrane PD-L1 is subject to proteolytic cleavage by ADAM10 and ADAM17 in breast cancer cells and in the normal epithelial cell line MCF10A. Importantly, selective up-regulation of ADAM10 activity upon treatment of cells with a calcium ionophore or stimulation of ADAM17 activity via phorbol ester-mediated activation of protein kinase C readily increases the release of sPD-L1. In the tumor microenvironment in vivo, intracellular calcium concentrations or protein kinase C activity may rise in response to a number of extracellular signals. Thus, although PD-L1 cleavage in unstimulated cells in vitro appears low and does not exceed 10% of the total cellular PD-L1, the cleavage in vivo may be considerably augmented by physiological stimuli in the tumor microenvironment.

Inhibition of sPD-L1 release in our experiments by chemical inhibitors or siRNAs targeting ADAM10 and ADAM17 did not exceeded ~80%. This could be partially due to incomplete inhibition of ADAM activity/expression, in particular incomplete elimination of ADAM10 by siRNAs (see Figure 2.6 a). However, we cannot rule out that other mechanisms also contributed to the release of sPD-L1, such as secretion of exosomal PD-L1 or cleavage by other proteases. When cells were incubated in the presence of serum, sedimentation of exosomes did not have a major effect on the measured levels of sPD-L1 in the media. However, after incubation of cells in serum-free media, some full-length PD-L1, in addition to the ~37-kDa fragment, was detected in the conditioned media (see Figure 2.3), suggesting that some exosomal PD-L1 might have contributed to the pool of PD-L1 in the media, at least under serum-free conditions.

Previous reports linked MMP-9 and MMP-13 to the cleavage of PD-L1 in fibroblasts and in head and neck carcinoma cells [57], [59]. However, these two MMPs are not highly expressed

in cells tested here, and thus are unlikely to mediate PD-L1 cleavage. Furthermore, MMP-9 and MMP-13 are secreted enzymes, and their substrates typically include components of the extracellular matrix, rather that transmembrane proteins [70]. ADAM10 and ADAM17 are, in contrast, membrane-bound proteases whose known substrates comprise transmembrane receptors, growth factor or cytokine precursors, and adhesion proteins [71], [72]. Notably, several ADAM10 and/or ADAM17 substrates contain two or more Ig-like domains and a membrane-proximal stalk region, for example, low-affinity IgγFc region receptor III (FcγRIII) [73], lymphocyte activation gene 3 protein (LAG-3) [74], or nectin-4 [75]. PD-L1, with two Ig domains, IgV and IgC, and a short stalk region connecting IgC to the transmembrane domain, is another example of this class of substrates.

ADAM10 or ADAM17-mediated cleavage of FcγRIII, LAG-3, and nectin-4 occurs in their membrane-proximal stalks. Based on our results, we propose that the metalloprotease cleavage site in PD-L1 is also located in the stalk region, between V225 and H240 (Figure 2.6 e). Cleavage of PD-L1-M/F within this region would generate two products of ~24 kDa and ~13 kDa (the N-terminal and C-terminal fragment, respectively). Since the extracellular domain of PD-L1 is glycosylated and ~12-15-kDa larger than the non-glycosylated form [48], the actual size of the N-terminal cleavage product would roughly correspond to the 37-kDa sPD-L1 identified here. The predicted size of the C-terminal cleavage product is smaller than the 18-kDa PD-L1-M/F fragment described here. This discrepancy may be due to abnormal mobility of this fragment in SDS-PAGE or it may be caused by PD-L1 mono-ubiquitination [47]. Since ADAMs do not recognize specific consensus sequences and their cleavage sites are poorly defined, additional studies are needed to determine the exact position of ADAM-mediated cleavage within PD-L1.

The C-terminal PD-L1 cleavage product appeared unstable in MDA-MB-231 and MCF10A cells. This result was somewhat unexpected in the context of recent studies, which identified CMTM6 and CMTM4, two MARVEL domain-containing transmembrane proteins, as critical regulators of PD-L1 stability [50], [51]. Biochemical characterization of CMTM6:PD-L1 complexes using PD-L1/PD-L2 chimeras suggested that the transmembrane domain of PD-L1 is required for the interaction with CMTM6 [51]. The C-terminal PD-L1 fragment observed here comprised the transmembrane domain of PD-L1 but, nevertheless, was significantly less stable than full-length PD-L1 in MDA-MB-231 and MCF10A cells. These results suggest that the presence of the transmembrane domain of PD-L1 is not sufficient for the interaction with CMTM6. This observation may have significant implications when designing methods to disrupt the interaction between PD-L1 and CMTM6, to destabilize PD-L1, and to overcome the immune evasion by tumor cells.

Interestingly, in BT549 cells, the C-terminal PD-L1 fragment appeared more stable and was detectable in the absence of lysosome inhibition (see Figure 2.4 and Supplementary Figure 2.1, Supplementary Figure 2.2, Supplementary Figure 2.3). According to the Catalogue Of Somatic Mutations In Cancer (COSMIC) database (https://cancer.sanger.ac.uk/cell_lines), BT549 cells carry a homozygous R438C mutation in the VPS18 gene (ENSG00000104142), and this mutation is predicted to be protein-damaging according to the SIFT and PolyPhen prediction tools available at the Ensembl genome browser (http://uswest.ensembl.org). Vacuolar protein sorting-associated protein 18 (VPS18) is a component of the mammalian homotypic fusion and vacuole protein sorting (HOPS) complex required for fusion of endosomes with lysosomes [76]. Thus, it is possible that increased stability of the C-terminal PD-L1 cleavage product generated

by ADAM10/17 is a consequence of its impaired delivery to lysosomes, but this hypothesis needs further testing.

An important question remains: what are the biological consequences of PD-L1 cleavage? Specifically, in the context of breast tumors in vivo, does the cleavage weaken or improve anti-tumor immunity? While a soluble extracellular domain of PD-L1 was reported to inhibit T cell responses in some circumstances [58], [77], it is generally believed that a soluble monomeric PD-L1 does not deliver a strong negative regulatory signal through PD-1. This is underscored by a recent discovery of a new secreted PD-L1 variant that has an ability to form homodimers through a Cys residue in its unique C-terminal tail and, unlike a monomeric soluble PD-L1, to inhibit lymphocyte function [55].

Instead, the cleavage of transmembrane PD-L1 may increase anti-tumor immunity, for example by reducing the amount of PD-L1 on tumor cells [57] or by providing sPD-L1 that competes with membrane-bound PD-L1 for PD-1. Furthermore, sPD-L1 may exert an immuno-stimulatory effect through its binding to CD80 (B7-1). While it has been previously established that, in addition to PD-1, PD-L1 also interacts with CD80 [78], recent studies have further demonstrated that PD-L1 and CD80 bind only in cis, on the same cell surface, in a parallel orientation [79]–[81]. CD80 homodimer, when not bound to PD-L1, interacts in trans with a co-inhibitory receptor CTLA4 or with a co-stimulatory receptor CD28 [82]. Remarkably, PD-L1:CD80 heterotrimer is unable to bind to PD-1 or CTLA4 on the neighboring cell, but binds to and activates CD28 equally well as free CD80 [81]. Thus, it is conceivable that sPD-L1 produced in one location within the tumor, with high local expression of transmembrane PD-L1 and high expression/activity of ADAM10 or ADAM17, diffuses to a different location where it binds to CD80 and switches it from a CTLA4 ligand to a CD28 ligand, effectively promoting T

cell activation. Importantly, such a function of sPD-L1 would not be mimicked by exosomal PD-L1, because the exosomal membrane would sterically prevent PD-L1 and CD80 to interact in a parallel orientation.

Finally, within the tumor microenvironment, ADAM10 and ADAM17 are expressed not only in cancer cells but also in tumor-infiltrating immune cells [71]. While we have not tested whether ADAM10 or ADAM17 might cleave PD-L1 in immune cells, the ubiquitous expression of these two ADAMs and regulation of their activities by a number of physiological signals clearly position them as new modulators of the PD-1/PD-L1 immune checkpoint pathway

.

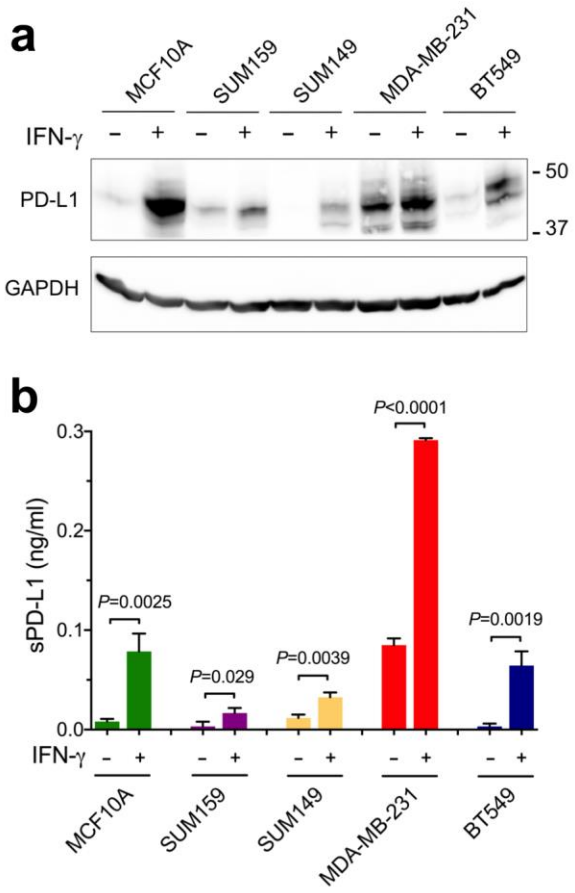

Figure 2.1 Interferon-γ increases PD-L1 protein levels in cell lysates and in culture media. Human breast cancer cells SUM159, SUM149, MDA-MB-231, BT549, and human non-transformed mammary epithelial cells MCF10A were incubated for 48 h without or with 10 ng/ml human IFN-γ. **a** Cell lysates were analyzed by Western blotting using anti-PD-L1 antibody (E1L3N). GAPDH is a gel loading control. **b** Concentrations of sPD-L1 in the media were measured by ELISA. Values are means ± S.D. from three replicate measurements, normalized to equal protein concentration in all cellular lysates. *P* values were determined by unpaired two-tailed Student's *t* test. Results in **a** and **b** are representative of three independent experiments

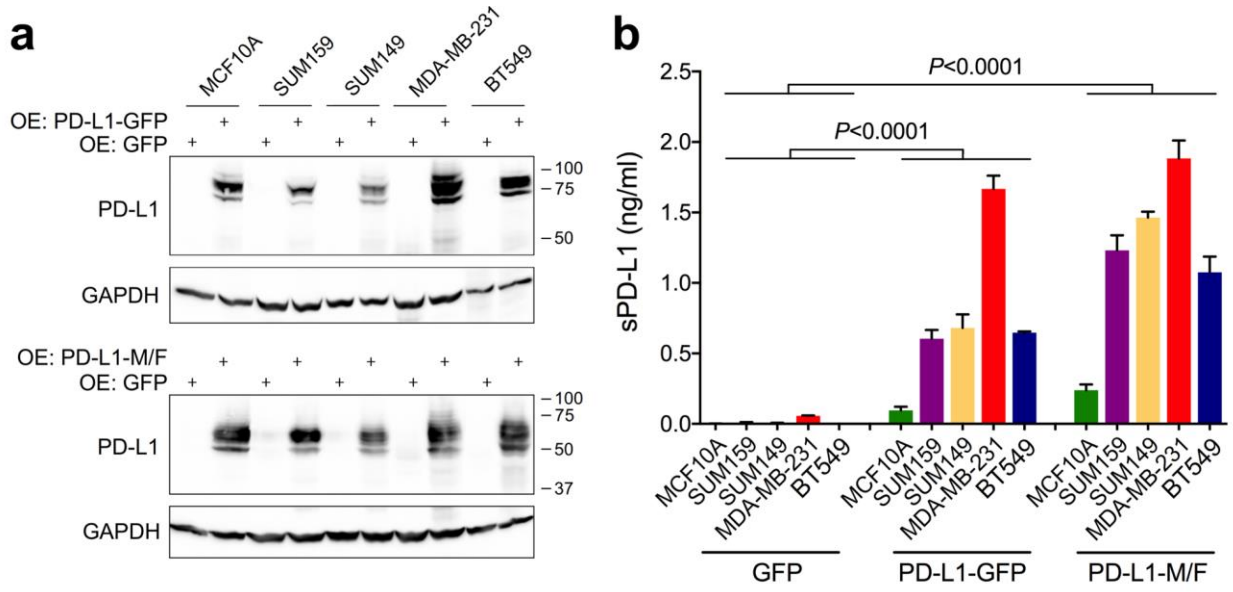

Figure 2.2 Elevated levels of soluble PD-L1 in culture media after stable overexpression of transmembrane PD-L1.

PD-L1-GFP, PD-L1-M/F, or GFP alone, were stably overexpressed in MCF10A, SUM159, SUM149, MDA-MB-231, and BT549 cells. **a** PD-L1 overexpression was confirmed by Western blotting using cell lysates and anti-PD-L1 antibody (E1L3N). Endogenous PD-L1 is not detectable at this exposure time. GAPDH is a gel loading control. **b** Concentrations of sPD-L1 in conditioned media were measured by ELISA. Values are means ± S.D. from three replicate measurements, normalized to equal protein concentration in all cell lysates. *P* value was determined by one-way ANOVA, followed by Tukey's multiple comparisons test. Results are representative of three independent experiments

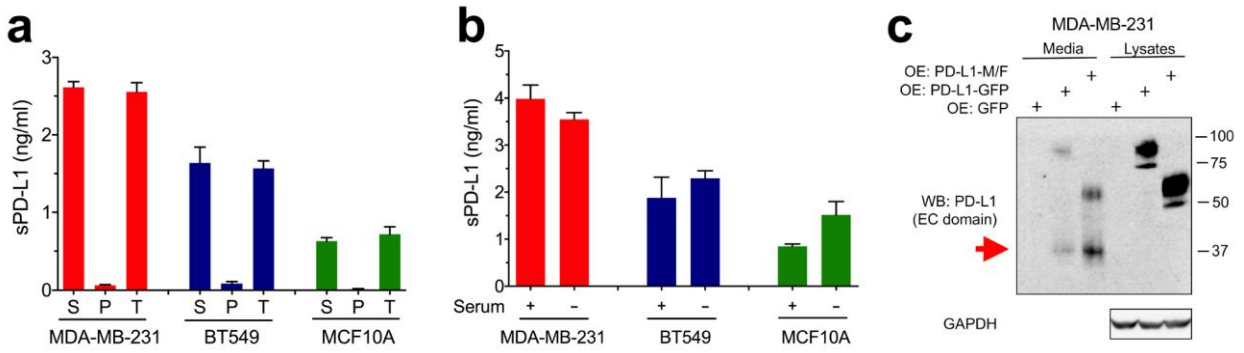

Figure 2.3 Soluble PD-L1 is generated by a proteolytic cleavage of transmembrane PD-L1. **a** Conditioned media from MDA-MB-231, BT549, or MCF10A cells with stable overexpression of PD-L1-M/F were centrifuged at 120,000xg for 1.5 h. sPD-L1 in the supernatants (S), pellets (P), and total media prior to centrifugation (T) was assayed by ELISA. Values are means ± S.D. from three replicate measurements. Results are representative of two independent experiments. **b** MDA-MB-231, BT549, or MCF10A cells stably overexpressing PD-L1-M/F were incubated for 24 h in media with or without serum. sPD-L1 in the media was assayed by ELISA. Values are means ± S.D. from three replicate measurements, normalized to equal protein concentration in all cellular lysates. Results in **a** and **b** are representative of three independent experiments. **c** MDA-MB-231 cells with stable overexpression of PD-L1-M/F, PD-L1-GFP, or GFP alone were incubated in serum-free media for 24 h. Conditioned media (70 μl, out of 1 ml of the total volume) or cell lysates (5 μl, out of 500 μl of the total volume) were analyzed by Western blotting using an antibody specific for the extracellular domain of PD-L1 (E1J2J). The N-terminal PD-L1 fragment detected in the media but not the lysates is indicated by red arrow. GAPDH is a gel loading control for lysate samples. Results are representative of two independent experiments

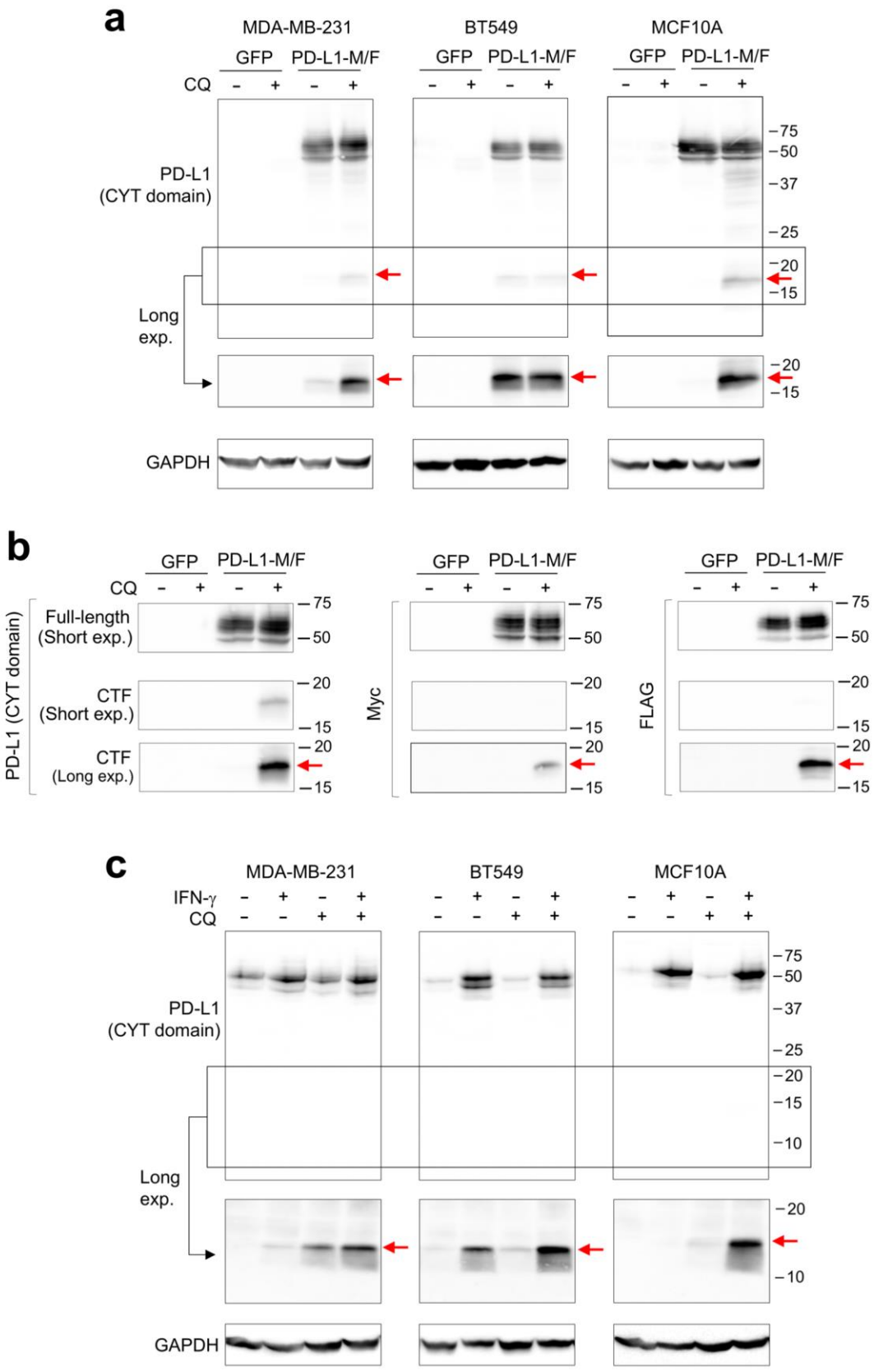
a
MDA-MB-231
BT549
MCF10A
GFP
PD-L1-M/F
CQ
PD-L1
(CYT domain)
Long
exp.
GAPDH
75
50
37
25
20
15
b
PD-L1 (CYT domain)
Full-length
(Short exp.)
CTF
(Short exp.)
CTF
(Long exp.)
Myc
FLAG
c
IFN-γ
CQ
PD-L1
(CYT domain)
Long
exp.
GAPDH
10

Figure 2.4 Detection of the C-terminal proteolytic fragment of PD-L1.

a MDA-MB-231, BT549, or MCF10A cells overexpressing PD-L1-M/F or GFP (control) were incubated for 24 h in the absence or presence of 10 μM chloroquine (CQ). Cell lysates were analyzed by Western blotting using an antibody specific for the cytoplasmic (CYT) domain of PD-L1 (E1L3N). The low-molecular weight region of the blot (indicated by the box) is also shown after a longer exposure time. **b** MDA-MB-231 cell lysates from panel **a** were analyzed by anti-PD-L1 (E1L3N), anti-Myc, or anti-FLAG antibody. Short and long exposures of the low-molecular weight region are shown. CTF, C-terminal fragment. (**c**) Parental MDA-MB-231, BT549, or MCF10A cells were incubated for 48 h in the presence or absence of 10 ng/ml IFN-γ, and then for additional 24 h with 10 μM CQ in the presence or absence of IFN-γ, as indicated. Cell lysates were analyzed by Western blotting using the E1L3N anti-PD-L1 antibody. The low-molecular weight region of the blot (indicated by the box) is also shown after a longer exposure time. GAPDH is a gel loading control. Results are representative of three (**a**) or two (**b, c**) independent experiments

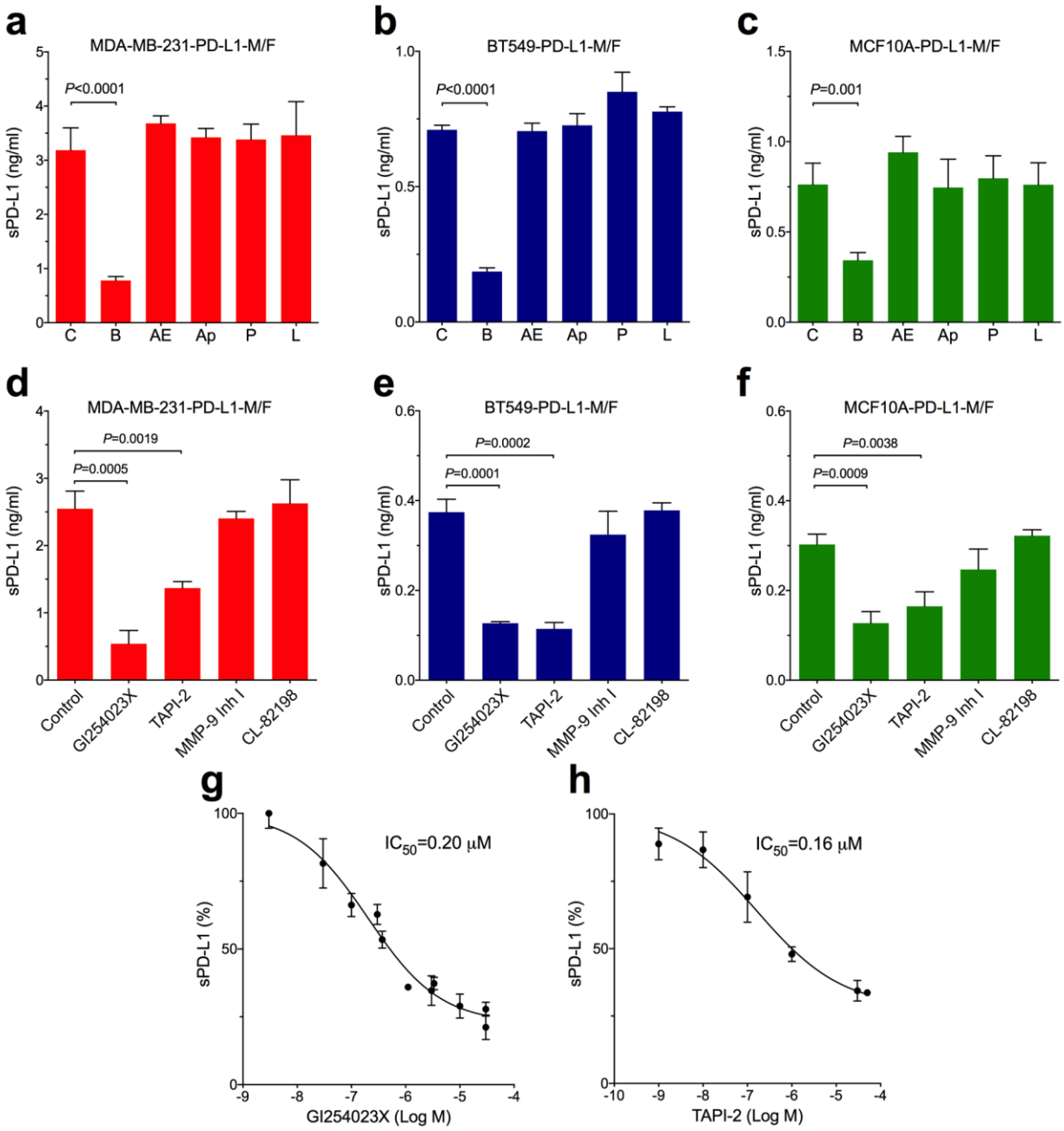

Figure 2.5 Cleavage of transmembrane PD-L1 is mediated by ADAM10 and ADAM17.

a MDA-MB-231, **b** BT549, or **c** MCF10A cells overexpressing PD-L1-M/F were incubated for 48 h in complete media containing 5 μM batimastat (B), 0.1 mM AEBSF (AE), 10 μg/ml aprotinin (Ap), 10 μg/ml pepstatin (P), 10 μg/ml leupeptin (L), or control media without inhibitors (C). **d** MDA-MB-231, **e** BT549, or **f** MCF10A cells overexpressing PD-L1-M/F were

incubated for 1 day in serum-free media containing 30 μM GI254023X, 30 μM TAPI-2, 50 μM MMP-9 Inhibitor I, 50 μM CL-82198, or control media without inhibitors. In **a**-**f**, concentrations of sPD-L1 in the media were measured by ELISA. Values are means ± S.D. from three replicate measurements, normalized to equal protein concentration in all cellular lysates. *P* values were determined by unpaired two-tailed Student's *t* test. Results are representative of three (**a, d**-**f**) or two (**b**, **c**) independent experiments. **g**, **h** MDA-MB-231-PD-L1-M/F cells were incubated for 1 day in serum-free media containing indicated concentrations of GI254023X (**g**) or TAPI-2 (**h**), followed by measuring sPD-L1 in the media by ELISA in triplicates. sPD-L1 concentrations in the absence of inhibitors were set at 100%. IC_{50} values for each inhibitor were determined after a non-linear regression curve fitting (four-parameter log(inhibitor) vs response) using GraphPad 6.0

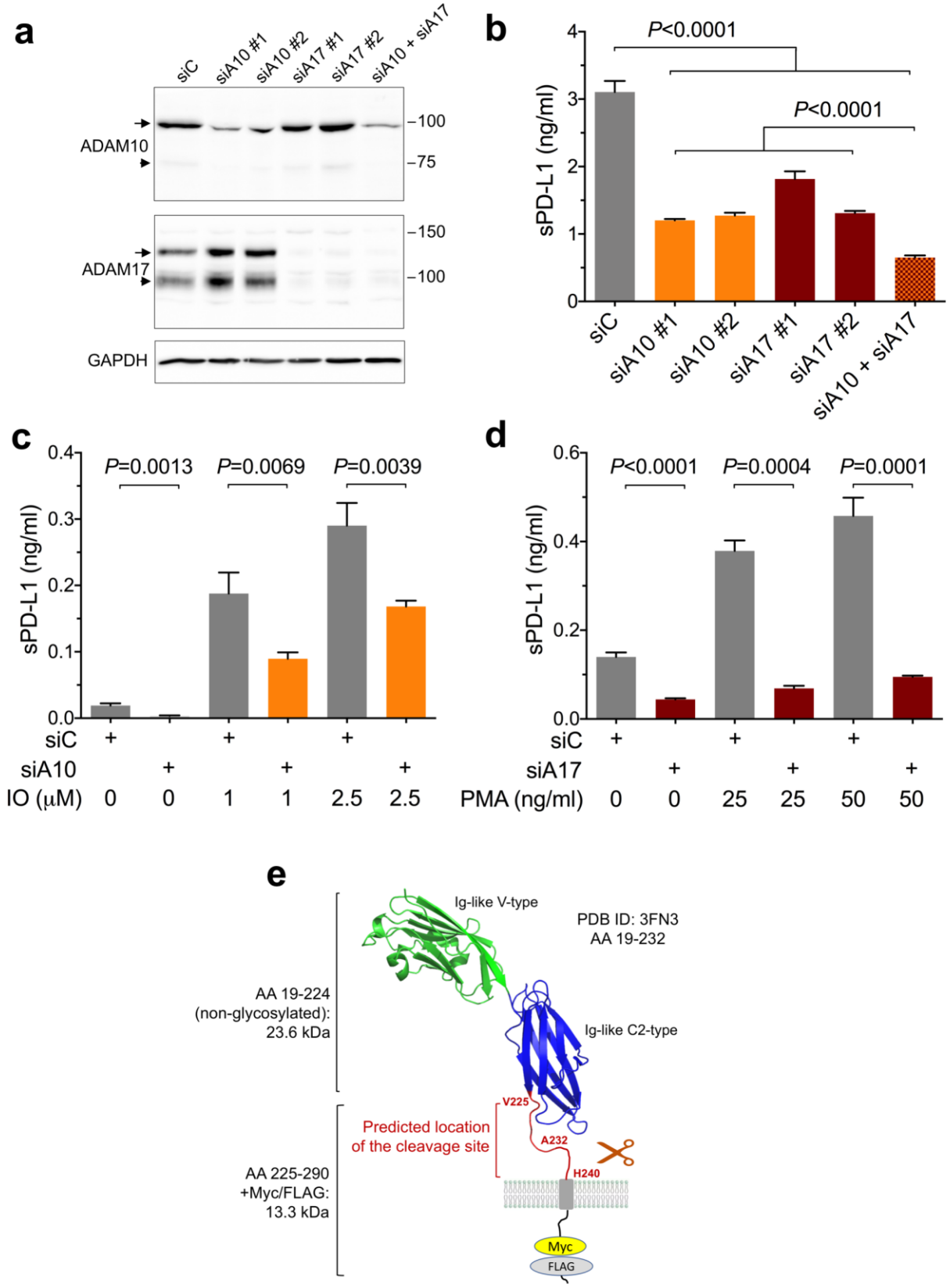
a
siC
siA10 #1
siA10 #2
siA17 #1
siA17 #2
siA10 + siA17
ADAM10
ADAM17
GAPDH
100
75
150
100
b
P<0.0001
P<0.0001
sPD-L1 (ng/ml)
c
P=0.0013
P=0.0069
P=0.0039
sPD-L1 (ng/ml)
siC
siA10
IO (μM)
d
P<0.0001
P=0.0004
P=0.0001
sPD-L1 (ng/ml)
siC
siA17
PMA (ng/ml)
e
Ig-like V-type
PDB ID: 3FN3
AA 19-232
AA 19-224
(non-glycosylated):
23.6 kDa
Ig-like C2-type
V225
Predicted location
of the cleavage site
A232
H240
AA 225-290
+Myc/FLAG:
13.3 kDa
Myc
FLAG

Figure 2.6 The effect of ADAM10 and ADAM17 knockdown on the cleavage of PD-L1. **a, b** MDA-MB-231-PD-L1-M/F cells were transfected with two different siRNAs targeting ADAM10 or ADAM17, a combination of all four siRNAs, or with control siRNA. Three days after transfection, ADAM10 and ADAM17 expression was analyzed by Western blotting (**a**), and concentrations of sPD-L1 in the media were measured by ELISA (**b**). Arrows, the nascent full-length ADAMs; arrowheads, the processed forms; GAPDH is a gel loading control. In **b**, values are means ± S.D. from three replicate measurements, normalized to equal protein concentration in all cellular lysates. *P* values were determined by one-way ANOVA, followed by Dunnett's multiple comparisons test. **c** MDA-MB-231-PD-L1-M/F cells were co-transfected with siRNA#1 and #2 targeting ADAM10 or with control siRNA. Two days after transfection, cells were incubated for 45 min in serum-free medium containing 0, 1 μM, or 2.5 μM ionomycin (IO), an activator of ADAM10, followed by ELISA for sPD-L1. **d** MDA-MB-231-PD-L1-M/F cells were co-transfected with siRNA#1 and #2 targeting ADAM17 or with control siRNA. Two days after transfection, cells were incubated for 2 h in complete medium containing 0, 25 ng/ml, or 50 ng/ml PMA, an activator of ADAM17, followed by measuring sPD-L1 by ELISA. Values are means ± S.D. from three replicate measurements. In **c** and **d**, *P* values were determined by unpaired two-tailed Student's *t* test. Results are representative of three (**b**) or two (**c, d**) independent experiments. **e** Predicted location of the cleavage site in PD-L1. The structure of human PD-L1 (aa 19-232, PDB ID: 3FN3) is shown. The Ig-like V-type domain is required for the interaction with PD-1. The membrane-proximal unstructured region between V225 and H240 most likely contains the metalloprotease cleavage site

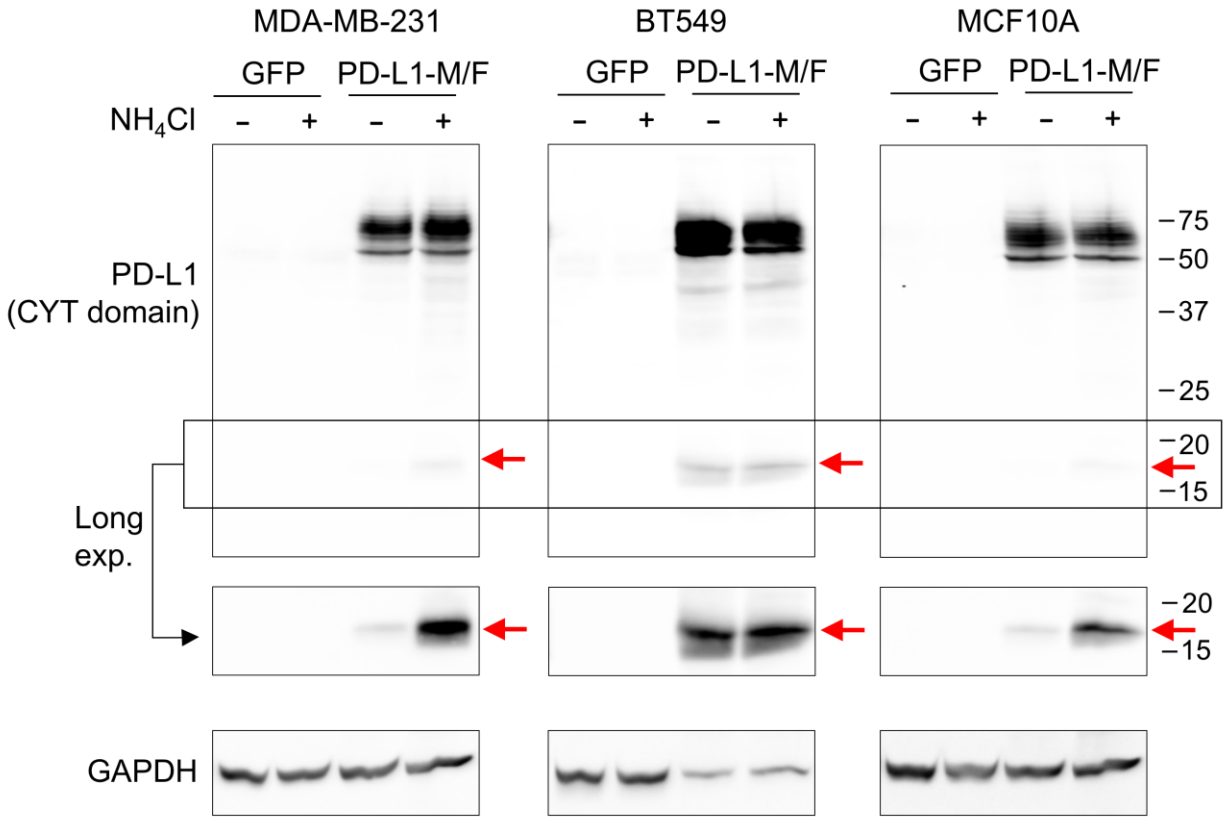

Supplementary Figure 2.1 The effect of ammonium chloride treatment on the C-terminal proteolytic fragment of PD-L1-M/F.

MDA-MB-231, BT549, or MCF10A cells overexpressing PD-L1-M/F or GFP (control) were incubated for 18 h in the absence or presence of 10 mM ammonium chloride (NH_4Cl). Cell lysates were analyzed by Western blotting using the E1L3N antibody specific for the cytoplasmic (CYT) domain of PD-L1. The low-molecular weight region of the blot (indicated by the box) is also shown after a longer exposure time. GAPDH is a gel loading control

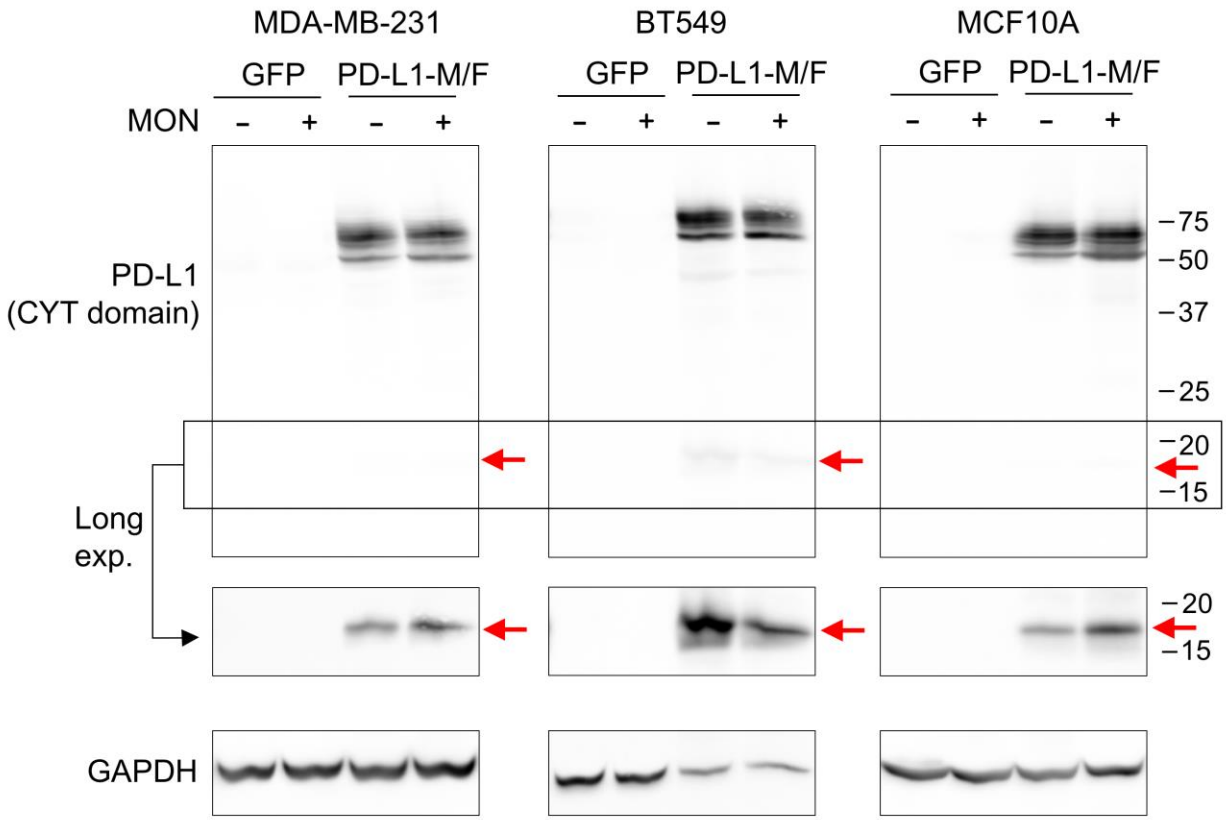

Supplementary Figure 2.2 The effect of monensin treatment on the C-terminal proteolytic fragment of PD-L1-M/F.

MDA-MB-231, BT549, or MCF10A cells overexpressing PD-L1-M/F or GFP (control) were incubated for 4 h in the absence or presence of 20 μM monensin (MON). Cell lysates were analyzed by Western blotting using the E1L3N antibody specific for the cytoplasmic (CYT) domain of PD-L1. The low-molecular weight region of the blot (indicated by the box) is also shown after a longer exposure time. GAPDH is a gel loading control

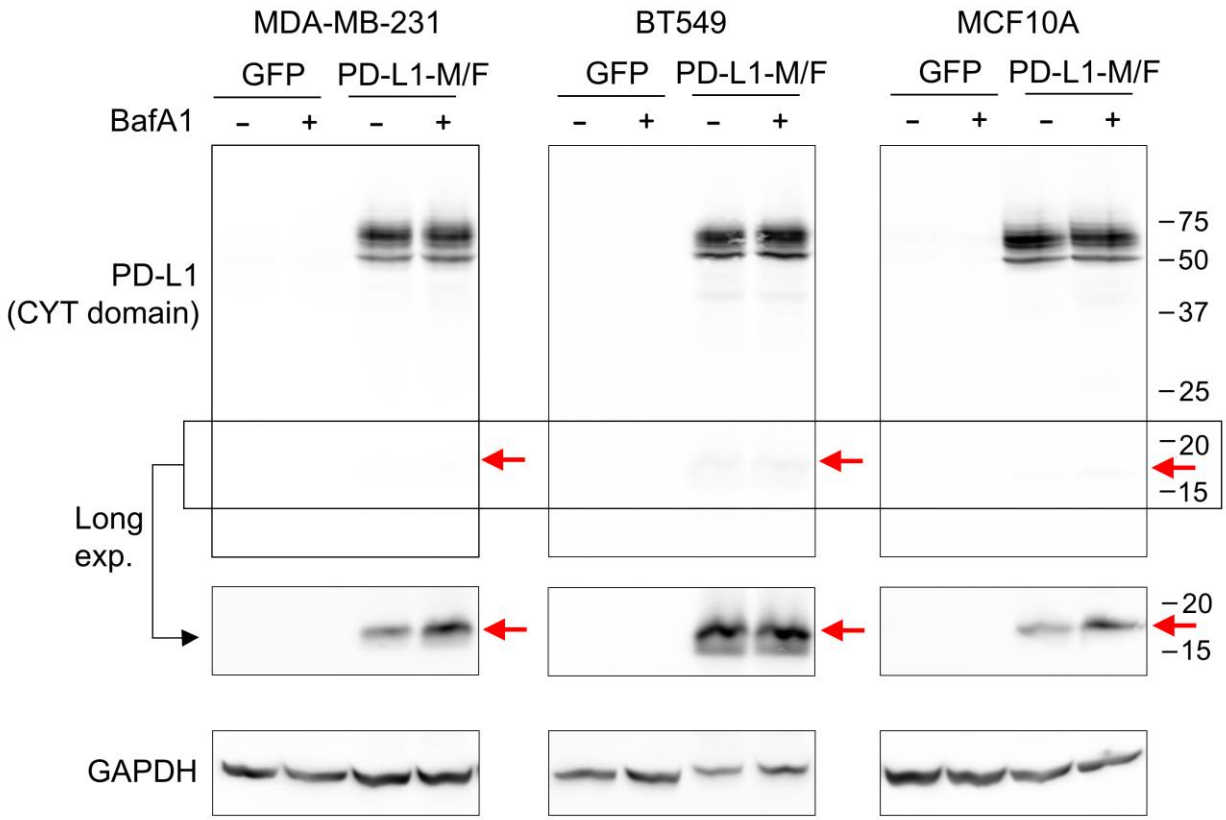

Supplementary Figure 2.3 The effect of bafilomycin A1 treatment on the C-terminal proteolytic fragment of PD-L1-M/F.

MDA-MB-231, BT549, or MCF10A cells overexpressing PD-L1-M/F or GFP (control) were incubated for 4 h in the absence or presence of 0.1 μM bafilomycin A1 (BafA1). Cell lysates were analyzed by Western blotting using the E1L3N antibody specific for the cytoplasmic (CYT) domain of PD-L1. The low-molecular weight region of the blot (indicated by the box) is also shown after a longer exposure time. GAPDH is a gel loading control

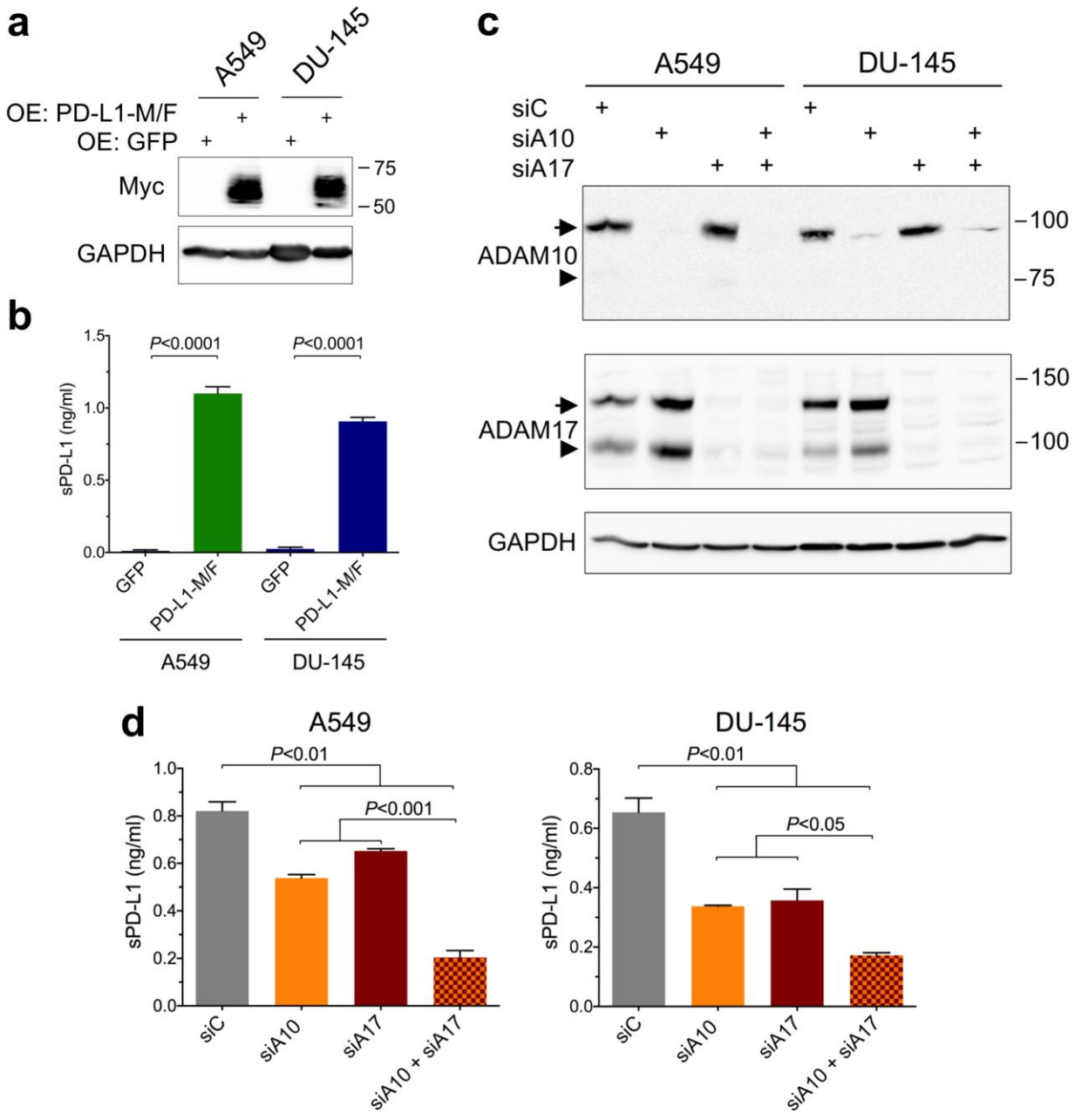

Supplementary Figure 2.4 The effect of ADAM10 or ADAM17 knockdown on the cleavage of PD-L1-M/F in non-breast cancer cell lines.

a A549 lung cancer cells and DU-145 prostate cancer cells were stably transduced to express PD-L1-M/F or GFP. PD-L1 overexpression was confirmed by Western blotting using total cell lysates and anti-Myc antibody. GAPDH is a gel loading control. **b** Concentrations of sPD-L1 in

the conditioned media were measured by ELISA. Values are means ± S.D. from three replicate measurements, normalized to equal protein concentration in all cell lysates. *P* values were determined by unpaired two-tailed Student's *t* test. **c**, **d** A549-PD-L1-M/F and DU-145-PD-L1-M/F cells were transfected with a mixture of siRNA#1 and #2 targeting ADAM10, a mixture of siRNA#1 and #2 targeting ADAM17, a combination of all four siRNAs targeting both ADAM10 and ADAM17, or with control siRNA. Three days after transfection, ADAM10 and ADAM17 expression levels were analyzed by Western blotting (**c**) and concentrations of sPD-L1 in the media were measured by ELISA (**d**). Arrows, the nascent full-length ADAMs; arrowheads, the processed forms. In **d**, values are means ± S.D. from duplicate measurements, normalized to equal protein concentration in all cellular lysates. *P* values were determined by one-way ANOVA, followed by Dunnett's multiple comparisons test. Results are representative of two independent experiments.

Chapter 3 - Role of ADAM12 in T Cell Accumulation in the Tumor Microenvironment

Abstract

Claudin-low breast tumors, an aggressive subtype often associated with the triple negative receptor status and poor patient prognosis, have been shown to have increased numbers of functional tumor-infiltrating Tregs. These Tregs lead to an immunosuppressive TIME and negatively impact immune checkpoint blockade response rates in patients. Claudin-low tumors also have upregulated expression levels of ADAM12, a catalytically active member of the ADAM family of cell surface metalloproteases which can catalyze the cleavage of many cancer related proteins. The goal of this study was to explore the relationship between ADAM12 and Treg accumulation in the TIME *in vivo*. Using a syngeneic T11 orthotopic cell transplantation mouse model and CRISPR/CAS9 mediated ADAM12 knockout, we show a significant increase of T cells, specifically Tregs, in claudin-low breast tumors lacking ADAM12. In contrast, there was no significant difference in the frequency of cytotoxic T cells, helper T cells, gamma delta T cells, natural killer T cells, dendritic cells and natural killer cells in the TIME in claudin-low breast tumors with or without expression of ADAM12. We postulate that this novel relationship between ADAM12 and Treg abundance in the TIME could have clinical implications and could be used to improve the outcome of immune checkpoint blockade therapies. However, further studies are necessary to determine the mechanism(s) by which ADAM12 influences Tregs accumulation.

Introduction

Claudin-low breast tumors make up a majority of triple-negative breast tumors and are characterized by a poor prognosis, high tumor grade, large tumor size and increased immune cell infiltration [7], [20]. The claudin-low subtype can be distinguished from the four other molecular subtypes by its increased expression of genes associated with epithelial-to-mesenchymal transition and stem cell-like characteristics [20], [83]. Recent studies have found that there is an increased expression of immune genes and increased numbers of tumor-infiltrating lymphocytes in claudin-low tumors [18], [20]. Specifically, claudin-low tumors were shown to have an increased infiltration of CD4+ T cells to the tumor site and focally increased numbers of Tregs [20]. Notably, infiltration of Tregs to the tumor site is often associated with resistance to immune checkpoint blockade therapy, specifically anti-PD-1 treatments [20], [84]. This is supported by the fact that claudin-low tumor-infiltrating Tregs are fully functional and capable of suppressing T cell responses [20]. When Treg depletion was combined with anti-PD-1 immune checkpoint blockade therapy, the authors saw decreased tumor growth, increased cytokine production by cytotoxic T cells and increased overall survival [20]. However, it is currently unknown why claudin-low breast tumors show high Treg infiltration.

Claudin-low tumors are also known to have high expression of a disintegrin and metalloprotease 12 (ADAM12) [28], [75]. ADAM12, an active member of the ADAM family of cell surface metalloproteases, is strongly upregulated in breast tumors and virtually not expressed in normal mammary epithelium [29], [37]. It is known to catalyze the cleavage of transmembrane receptors, growth factors and adhesion molecules, such as Notch receptors, epidermal growth factor receptor ligands and many other cancer related proteins [29]. Studies have also shown that ADAM12 is induced during epithelial-to-mesenchymal transition, a feature

specific to claudin-low breast tumors [29]. Here, we postulate that ADAM12 may mediate the release of a number of growth factors and cytokines from tumor cells, which could facilitate Treg accumulation or regulate their properties. If a relationship is established between ADAM12 and Treg accumulation, therapies targeting ADAM12 could prove to be beneficial in the attempt to deplete Tregs from the TIME and thus reactivate the immune response against cancer cells.

The goal of this study was to explore the role of ADAM12 in T cell accumulation to the tumor microenvironment *in vivo*. Specifically, I investigated the accumulation of regulatory T cells, cytotoxic T cells, gamma delta T cells, helper T cells and natural killer T cells to the tumor microenvironment in a mouse model of claudin-low cancer. We utilized an orthotopic cell transplantation model, in which T11 cells were injected into mammary glands of Balb/cJ mice. The T11 cell line is a p53-null mouse breast cancer cell line which, when injected into mice, forms claudin-low tumors that closely mimic human claudin-low tumor biology, including high content of Tregs [20], [86]. By utilizing this model and performing ADAM12 knockout in T11 cells, we were able to determine that the frequency of Tregs among tumor-infiltrating immune cells was increased upon loss of ADAM12 expression.

Materials and Methods

Antibodies and Reagents

Reagent or Resource	Source	Identifier
Antibodies		
FITC-conjugated anti-CD45 (clone 30-F11)	Biolegend	Cat # 103107
Rat IgG2b, κ isotype control (clone RTK4530)	Biolegend	Cat # 400605
Alexa Fluor 700-conjugated anti-CD3 (clone 17A2)	Biolegend	Cat # 100215
Rat IgG2b κ isotype control (clone RTK4530)	Biolegend	Cat # 400628
PE/Cyanine7-conjugated anti-CD8a (clone 53-6.7)	Biolegend	Cat # 100721
PE-conjugated anti-CD8a (clone 53-6.7)	Biolegend	Cat # 100707
Rat IgG2a κ isotype control (clone RTK2758)	Biolegend	Cat # 400507
Brilliant Violet 785-conjugated anti-CD4 (clone RM4-5)	Biolegend	Cat # 100551
Rat IgG2a κ isotype control (clone RTK2758)	Biolegend	Cat # 400546
APC-conjugated anti-CD11c (clone N418)	Biolegend	Cat # 117309
Armenian Hamster IgG isotype control (clone HTK888)	Biolegend	Cat # 400911
APC-conjugated anti-CD4 (clone RM4-5)	Biolegend	Cat # 100516
Rat IgG2a κ isotype control (clone RTK2758)	Biolegend	Cat # 400511
Alexa Fluor 488-conjugated anti-CD25 (clone PC61)	Biolegend	Cat # 102017
Pacific Blue-conjugated anti-CD45 (clone 30-F11)	Biolegend	Cat # 103125
PE-conjugated anti-CD25 (clone PC61)	Biolegend	Cat # 102008
Rat IgG1 λ isotype control (clone G0114F7)	Biolegend	Cat # 401906
Alexa Fluor 647-conjugated anti-FOXP3 (clone MF-14)	Biolegend	Cat # 126408
Rat IgG2b κ isotype control (clone RTK4530)	Biolegend	Cat # 400626
APC-conjugated anti-TCR γ/δ (clone GL3)	Biolegend	Cat # 118116
PE/Cyanine7-conjugated anti-CD49b (clone DX5)	Biolegend	Cat # 108922
TruStain FcX Plus anti-CD16/32 (clone S17011E)	Biolegend	Cat # 156603
Rabbit polyclonal anti-ADAM12 antibody raised against amino acid 774-791 of the cytoplasmic tail of mouse ADAM12	[85]	# 5114-2
Reagents		
Precision Count Beads	Biolegend	Cat # 424902
Propidium Iodine Staining Solution	BD Pharmingen	Cat # 556463
Zombie NIR Fixable Viability Kit	Biolegend	Cat # 423105
Fixable Viability Dye eFluor 450	Thermo Fisher Scientific	Cat # 65-0863
True Nuclear transcription factor buffer set	Biolegend	Cat # 424401
Cyto-Last Buffer	Biolegend	Cat # 422501
KN2.0, non-homology mediated CRISPR/Cas9 knockout kit	OriGene	Cat # KN508813
Turbofectin 8.0	OriGene	Cat # TF81001
Transforming growth factor beta	R&D Systems	Cat # 240-B-002
Concanavalin A Sepharose	GE Healthcare	Cat # C7555
Fetal Bovine Serum	Corning	Cat # MT35015CV
Bovine Serum Albumin	Amresco	Cat # 9048-46-8

Table 3.1 Antibodies and Reagents

Cell Culture

The T11 cell-line was provided by Dr. Jeff Rosen (Baylor College of Medicine) [20]. T11 cells were cultured in Dulbecco's modified Eagle's medium (DMEM) supplemented with 10% fetal bovine serum. Cells were maintained at 37 °C in the presence of 5% CO_2 under a humidified atmosphere.

Prior to concanavalin A sepharose purification of ADAM12 from T11 cells (wildtype or ADAM12 KO), cells were incubated with 5 ng/mL transforming growth factor β (TGF-β) for 48 hours.

Concanavalin A Sepharose Purification of ADAM12

Cells were incubated for 15 min with lysis buffer containing 50 mM Tris-HCL pH 7.4, 150 mM NaCl, 1% Triton X-100, 1 mM $CaCl_2$, 1 mM $MgCl_2$, 1 mM (2-Aminoethyl) benzenesulfonyl fluoride hydrochloride (AEBSF), 10 µg/mL pepstatin, 10 µg/mL leupeptin, 10 µg/mL aprotinin, and 10 mM 1,10-phenanthroline. Cell extracts were centrifuged for 15 minutes at 13,000 rpm at 4°C. Supernatants (1.4 mL) were incubated with 20 µL concanavalin A sepharose for 4 hours at 4°C to enrich for glycoproteins. The sepharose beads were then washed three times with lysis buffer, bound glycoproteins were eluted with 3X SDS buffer, and subjected to analysis by immunoblotting, as described below.

Establishment of ADAM12 Knockout in T11 Mouse Breast Cancer Cell Line

T11 ADAM12 knockout cell lines were produced using KN2.0 non-homology mediated CRISPR/Cas9 knockout kit (OriGene). Briefly, T11 cells were seeded in 6-well plates (~$3x10^5$ cells per well). After 24 h, cells were co-transfected with one of the pCas-Guide CRISPR vectors and the linear donor DNA containing LoxP-EF1A-BFP-P2A-Neo-LoxP cassette, according to Origene CRISPR/Cas9 Knockout kit manual. Forty-eight hours post-transfection, cells were split

at a ratio of 1:10 and continued to grow for one week prior to the selection with 1 µg/mL G418 for 10 days.

Single cell colonies of G418-selected cells were isolated using two methods: limiting dilution and cloning cylinders. Limiting dilution: cells were diluted to ~10 cells/ml, and 100 µL of cell suspension was plated into wells in a 96-well plate. After 1-2 weeks, wells were observed under the microscope and wells containing only one cell colony were further expanded to 24-well plates and subsequently to 6-well plates. Individual clones were then subjected to flow cytometry and Western blot analysis. Cloning cylinders: ~10 cells were seeded in a 100 mm^2 plate. After 1-2 weeks, glass cylinders were placed around single cell colonies using grease to firmly attach cylinders to the plates. Colonies in the cylinders were trypsinized and directly transferred to wells in a 6-well plate. After expansion, cells from individual wells were subjected to flow cytometry and Western blot analysis.

Immunoblotting

Cellular proteins were resolved by SDS-PAGE and transferred to a nitrocellulose membrane. The membrane was blocked with 5% milk in Dulbecco's Phosphate Buffered Saline (DPBS) containing 0.3% Tween-20. Rabbit polyclonal anti-ADAM12 antibody was diluted 1:1,000 in blocking buffer and incubated with the membrane overnight at 4°C. Horseradish peroxidase-conjugated anti-rabbit IgG antibody was used as the secondary antibody at a dilution of 1:5,000 and incubated with the membrane for one hour. Signal detection was performed using SuperSignal West Pico Chemiluminescent kit (Pierce) and Azure c500 digital imaging system.

Mice Injections

All animals had free access to food and water and were exposed to a 12-hour light/dark cycle. Animal experiments were conducted in compliance with the protocol #4119 approved by

the Institutional Animal Care and Use Committee. Balb/cJ 6-7-week-old female mice were purchased from The Jackson Laboratory, 8-12-week-old mice were used for all experiments. Wild-type or ADAM12 KO cells were trypsinized into single cell suspensions, counted, and resuspended in PBS at a density of $2x10^5$ cells/mL. Mice were anesthetized with 3% isoflurane inhalation and 50 µL of cell suspension ($1x10^4$ cells) was injected into the 4^{th} inguinal mammary fat pad using a 1 mL tuberculin syringe with a 5/8-inch 25-gauge needle. Mice were monitored daily and tumor growth was measured with a caliper. Mice were sacrificed and tumors were harvested when the tumor size reached ~100 mm^2 (length x width), or after ~28 days, whichever occurred earlier.

Isolation of Tumor Infiltrating Lymphocytes

Mice bearing T11 tumors (wild-type or ADAM12 KO) were sacrificed and tumors were resected. Tumors were then placed in 5 mL Hank's balanced salt solution with calcium and magnesium (Lonza) at room temperature and cut with razor blades, and then chemically digested in (10 mg/mL) Collagenase type IV (Sigma-Aldrich), (200 units/mL) DNase type IV (Sigma-Aldrich) and (1,500 units/mL) Hyaluronidase type IV-S (Sigma-Aldrich) at room temperature for 1 hour with shaking at 130 rpm. Single cell suspension was obtained by passing the solution through a 70-µm nylon mesh cell strainer (Fisher Scientific). Chemical digestion was stopped by adding 1 mM EDTA followed by centrifugation and discarding of supernatants. The cell suspension was briefly incubated in ACK lysing buffer (Lonza) to deplete red blood cells then washed with PBS without calcium or magnesium. Cell suspensions were enriched for lymphocytes by centrifugation in a 42% and 78% Percoll (GE Healthcare) gradient in DMEM medium, at 1000 x g for 20 mins with no brake on the deceleration. After centrifugation, ~ 2 ml of the solution containing leukocytes at the interface between two Percoll concentrations was

collected. Isolated lymphocytes were washed with PBS without calcium or magnesium and resuspended in flow cytometry staining buffer (FACS Buffer, containing PBS and 3% bovine serum albumin).

Flow Cytometry

Cells in FACS buffer were blocked with TruStain FcX Plus (2.5 µg/mL) for 10 minutes on ice. Cells were then incubated with fluorochrome-labeled antibodies or their respective isotype antibody controls for 30 minutes on ice. In some experiments, Precision Count Beads were added to obtain absolute counts of cells acquired. Following a wash with FACS buffer, cells were resuspended in 400 µL of FACS buffer, supplemented with (1 µg/mL) of propidium iodide (PI) viability dye, and analyzed with an LSR Fortessa X-20 flow cytometer. For intracellular staining with FOXP3 antibody: Cells in 1 mL PBS without calcium or magnesium were incubated with 1 µL Fixable Viability Dye for 30 minutes in the dark, on ice. Following a wash with FACS buffer, cells were blocked in FACS buffer with TruStain FcX Plus (2.5 µg/mL) for 10 minutes on ice. Cells were then incubated with surface marker fluorochrome-labeled antibodies or their respective isotype antibody controls for 30 minutes on ice. Following a wash with FACS buffer, cells were incubated in 1 mL True Nuclear 1X Fix in the dark at room temperature for 1 hour. After centrifugation, cells were resuspended in 0.5 mL Cyto-Last buffer, capped and stored at 4 °C in the dark until the next day. The following day, Cyto-Last buffer was removed by centrifugation. Without washing, cells were resuspended in 2 mL of True Nuclear 1X Perm Buffer. Following centrifugation, cells were washed again in 2 mL of True Nuclear 1X Perm Buffer. Cells were then incubated in 100 µL True Nuclear 1X Perm Buffer with 10 µg/mL intracellular staining FOXP3 antibody for 30 minutes in the dark at room temperature. After centrifugation, cells were resuspended in 2 mL of True Nuclear 1X Perm Buffer. Following a

wash with FACS buffer, cells were resuspended in 400 µL of FACS buffer and analyzed with an LSR Fortessa X-20 flow cytometer. Data were analyzed with FCS Express 6 (DeNovo Software). Gates were drawn based on fluorescence minus one-controls and isotype controls. Only viable cells were included in the analysis.

Results

Previously it was reported that ADAM12 is upregulated in claudin-low breast cancer, which is characterized by high immune cell infiltration, specifically by elevated numbers of Tregs [7], [37], [38]. Therefore, we set out to explore the relationship between ADAM12 and the accumulation of T cells, in particular Tregs, in the tumor immune microenvironment.

A commercially available non-homology mediated CRISPR/Cas9 knockout kit was used to develop an *Adam12* gene knockout in T11 mouse breast cancer cell line, as described in Methods. T11 cells were co-transfected with a pCas-Guide CRISPR vector targeting *Adam12* and the linear donor DNA containing the LoxP-EF1A-BFP-P2A-Neo-LoxP cassette. After selection with G418, several single cell colonies were isolated and analyzed by flow cytometry to identify clones expressing blue fluorescent protein (BFP), a reporter signal for knockout (Figure 3.1). To further validate the loss of ADAM12 expression in BFP+ clones, cells were subjected to Western blot analysis. Since the *Adam12* gene is known to be regulated by TGF beta [32], cells were incubated for 2 days with or without TGF beta prior to the analysis to positively identify ADAM12 bands (a ~120-kDa full-length form and a ~100-kDa mature form) (Figure 3.2). At the end, a single ADAM12 KO clone was selected for future experiments based on BFP sorting and Western blot results (Figure 3.2).

In vitro analysis of wild-type and ADAM12 KO T11 cells was performed to compare cell growth. Cells were counted and seeded at identical starting concentrations in 100 mm^2 plates. Cell concentrations were then determined at different time points between 0 and 72 hours (0, 16, 24, 40, 48, 64, 72 hours) after plating. Comparison of wild-type T11 and ADAM12 KO growth curves showed no significant difference between the two cell types (Figure 3.3). However, a comparison of *in vivo* tumor growth between wild-type and ADAM12 KO cells showed a clear

difference in growth rates. We found that tumors formed by ADAM12 T11 KO cells grew slower than tumors formed by wild-type T11 cells (Figure 3.4). Similarly, previous studies have shown that ADAM12 knock-down in human breast cancer cell line SUM159 led to slower tumor growth after injection into immunocompromised mice [29]. Thus, the slower tumor growth after ADAM12 downregulation does not seem to involve the immune system.

We next explored the consequences of ADAM12 KO in T11 tumor cells on the recruitment of immune cells to the tumor microenvironment. Briefly, mice were injected with 1 x 10^4 T11 (wildtype or ADAM12 KO) tumor cells. Tumors were then harvested when their size reached ~100 mm^2, or after 28 days, chemically digested, enriched for lymphocytes via Percoll density gradient centrifugation, and analyzed by flow cytometry for determination of the absolute number of leukocytes. Flow cytometry analysis gating strategies are shown in Supplementary Figure 3.1. Using the CD45+ as a leukocyte cell surface marker, we found that there was a slight increase in the absolute numbers of leukocytes per gram of tumor tissue in ADAM12 KO tumors compared to control tumors, but this difference was not statistically significant (Figure 3.5).

We then further analyzed subpopulations of tumor-infiltrating CD45+ cells, including CD45+CD3+ cells (T cells), CD45+CD49b+CD3- cells (NK cells) and CD45+CD11c+CD3- cells (dendritic cells). Multicolor flow cytometry analysis showed a statistically significant increase in the frequency of CD3+ T cells among CD45+ cells in ADAM12 KO tumors (Figure 3.6 a). In contrast, we did not find any differences in the CD45+CD49b+CD3- and CD45+CD11c+CD3- cells between wild-type and ADAM12 KO tumors (Figure 3.6 b & c). Together these results suggest that although the total leukocyte cell numbers are not significantly increased, specific subpopulations of leukocytes, namely T cells, are increased.

Next, we further characterized the subpopulations of tumor-infiltrating CD45+CD3+ T cells. We examined the percent of CD4+CD8- (helper and regulatory T cells), CD8+CD4- (cytotoxic T cells), CD49b+ (NKT cells) and TCRγδ+ (γδ T cells) cells. Examples of gating strategies for CD4+CD8- and CD8+CD4- populations are shown in Supplementary Figure 3.2. We found that there was no significant difference in CD8+CD4- or TCRγδ+ subpopulations between wild-type and ADAM12 KO tumors (Figure 3.7 a, b, c, d). We noticed a slight increase in the frequency of CD4+CD8- T cells and NKT cells in ADAM12 KO tumors, but this increase was not significant (Figure 3.7 a & c).

Finally, because T11 tumors are known to contain increased numbers of Tregs [20], we investigated the percent of Tregs in wild-type and ADAM12 KO tumors. Tregs were defined as CD45+CD3+CD4+CD25+FOXP3+ cells [8] and flow cytometry analysis gating strategies are shown in Supplementary Figure 3.3. Our data showed that there was a significantly higher frequency of Tregs among CD4+CD3+ T cells, among all CD3+ T cells, and among all CD45+ leukocytes in ADAM12 KO tumors than in wild-type tumors (Figure 3.8 a, b, c). Collectively, these results indicate that ADAM12 plays a role in the accumulation of T cells, more specifically, Tregs to the tumor immune microenvironment, and that the absence of ADAM12 in tumors leads to increased presence of Tregs in the tumor microenvironment.

Discussion

Even though it is known that claudin-low tumors have high infiltration of functional Tregs which contribute to the immunosuppressive tumor microenvironment [20], [84], the lack of knowledge about the mechanisms by which these Tregs accumulate in the TIME prevents the development of selective anti-Treg immunotherapies. Conventional methods which systemically target and deplete Tregs pose a significant problem because they lead to inflammatory and immune-related adverse events [84]. While some studies have suggested that soluble proteins, such as the chemokine CXCL12 [20], are involved in the recruitment of Tregs to the claudin-low tumor site, we hypothesized that ADAM12 could also play a role in this process. Our rationale was based on the notion that ADAM12 is an active proteolytic enzyme which can cleave and release soluble factors that could be involved in the recruitment of Tregs. Furthermore, both Tregs and ADAM12 are upregulated in claudin-low tumors, a trend that is not seen for other ADAMs. Therefore, we reasoned that if a relationship is established between ADAM12 expression and Treg accumulation, new therapies could target ADAM12 rather than Tregs themselves, limiting unwanted side effects that accompany anti-Treg treatments.

Although *in vitro* analysis showed no significant difference between the growth rates of wild-type and ADAM12 KO T11 cells, our *in vivo* experiments demonstrated notable differences between the growth rates of wild-type and ADAM12 KO tumors. We found that ADAM12 KO T11 tumors grew slower than tumors formed by wild-type T11 cells. This result is consistent with previous studies showing that ADAM12 knock-down in human breast cancer cells SUM159 led to slower tumor growth following transplantation into immunocompromised mice [29]. Thus, slower growth of ADAM12 KO T11 tumors may be an inherent trait of cancer cells, not influenced by the immune system or TIME.

Here, we show that there was a slight increase in the absolute numbers of CD45+ leukocytes per gram of tumor tissue in ADAM12 KO claudin-low tumors compared to control tumors, but this difference was not statistically significant. We did, however, show a statistically significant increase in the frequency of CD3+ T cells among CD45+ cells in ADAM12 KO tumors.

Importantly, we found that there was a significantly higher frequency of Tregs among CD4+CD3+ T cells, among all CD3+ T cells, and among all CD45+ leukocytes in ADAM12 KO tumors when compared to wild-type tumors. These results show that ADAM12 does play a role in the accumulation of Tregs into the TIME and suggest a negative correlation between ADAM12 and Treg infiltration. Although these results are unexpected, they are nevertheless important and can have potential clinical implications.

Based on our results, it can be proposed that manipulations to increase ADAM12 protein levels in claudin-low tumors may decrease Treg tumor infiltration and reactivate antitumor immunity. This could be achieved, for example, by using known inducers of ADAM12 expression, including TGF beta or Notch signaling [32], [33]. Furthermore, additional experiments should be done to test whether combining upregulation of ADAM12 with anti-PD-1/PD-L1 immune checkpoint blockade therapy would improve the effect of anti-PD-1/PD-L1 treatment on tumor growth, cytotoxic T cell cytokine production and overall survival in T11 mice models.

Finally, an important question remains: what is the mechanism(s) by which ADAM12 expression is negatively correlated with Treg infiltration in claudin-low tumors? We speculate that ADAM12 could mediate the cleavage and release of certain factors that could act on Tregs to block their migration to the TIME. Therefore, ADAM12 knockout would result in decreased

levels of factors blocking Treg infiltration and, in consequence, increased frequency of Tregs in the tumors. This idea is consistent with the fact that ADAMs are responsible for the release of soluble factors that influence cell migration. Alternatively, ADAM12 may deactivate, via cleavage, soluble factors that act as chemoattractants of Tregs. Given the critical immunosuppressive role of Tregs in the TIME and their negative effects on the response rates to immune checkpoint blockade therapy in TNBC, the relationship between ADAM12 and Treg accumulation should be investigated in more detail to improve the existing immunotherapies as well as to facilitate the development of new targeted therapies.

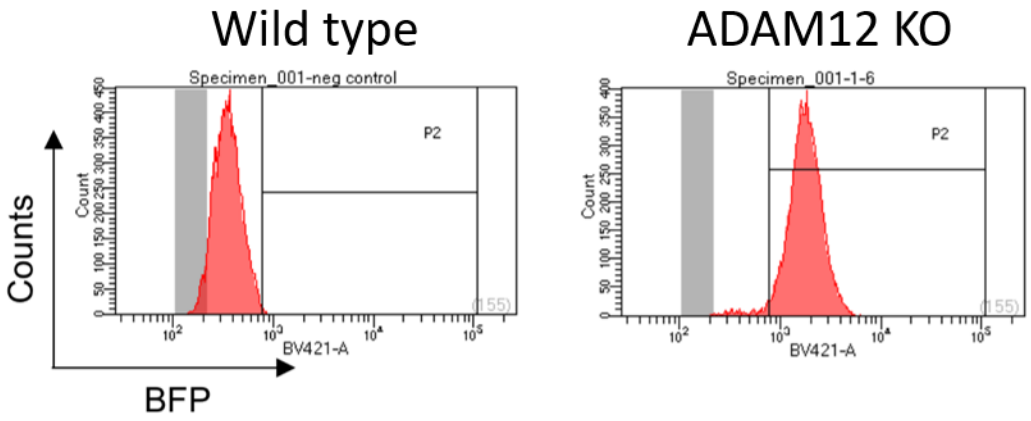

Figure 3.1 Verification of donor integration during CRISPR/Cas9 by flow cytometry

T11 cells were co-transfected with one of the pCas-Guide CRISPR vectors and the linear donor DNA containing the LoxP-EF1A-BFP-P2A-Neo-LoxP cassette. Stable transfectants were selected in the presence of neomycin. The expression level of BFP, a reporter for donor integration, in parental wild-type T11 cells and in ADAM12 KO cells was analyzed by flow cytometry.

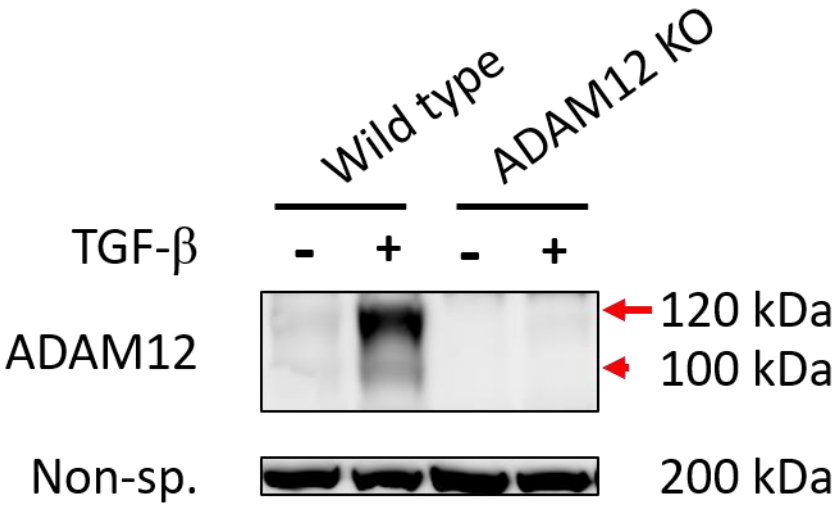

Figure 3.2 Verification of ADAM12 KO in T11 cells by Western blotting

Wild-type or ADAM12 KO T11 cells were cultured in the absence or presence of 5 ng/mL TGF-beta for 48 hours. Cells were lysed and ADAM12 was partially purified using Concanavalin A agarose beads. Shown are Western blots of the eluates from Concanavalin A agarose using anti-ADAM12 antibody. The nascent full-length ADAM12 is shown with arrow, the mature proteolytically processed ADAM12 is shown with arrowhead. A non-specific band served as a loading control.

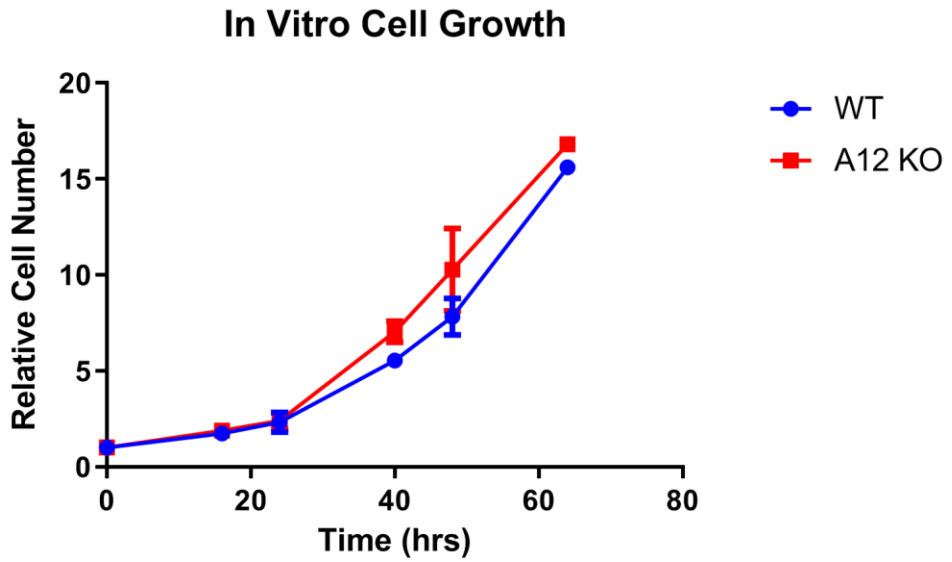

Figure 3.3 *In vitro* cell growth curve of wild-type and ADAM12 KO T11 cells

Wild-type or ADAM12 KO T11 cells were cultured *in vitro* in 100 mm^2 plates and cell numbers were determined at different time points between 0 and 72 hours after plating.

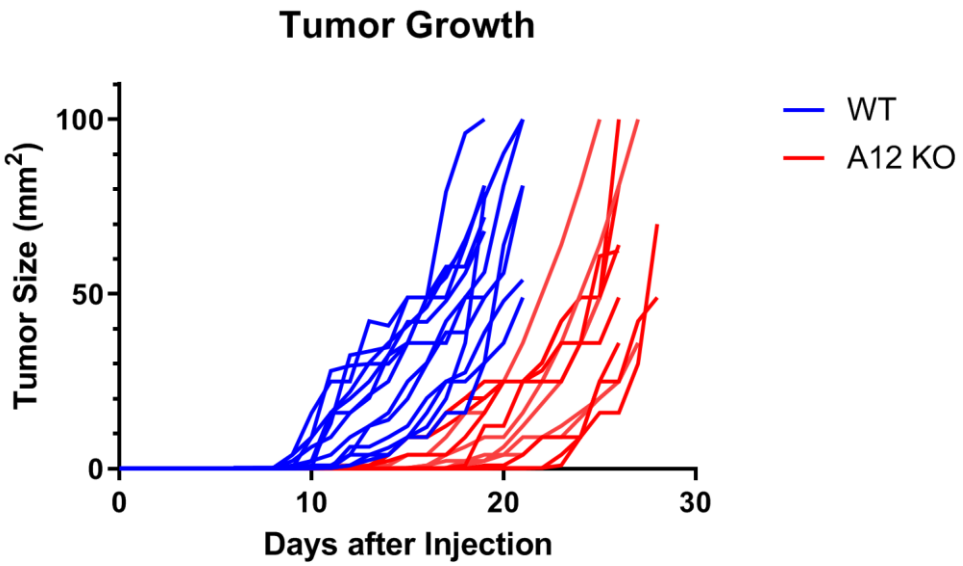

Figure 3.4 *In vivo* growth curves for wild-type and ADAM12 KO tumors

Wild-type or ADAM12 KO T11 cells (1 x 10^4 cells) were orthotopically injected into Balb/cJ mice. Tumor sizes were measured daily with a caliper.

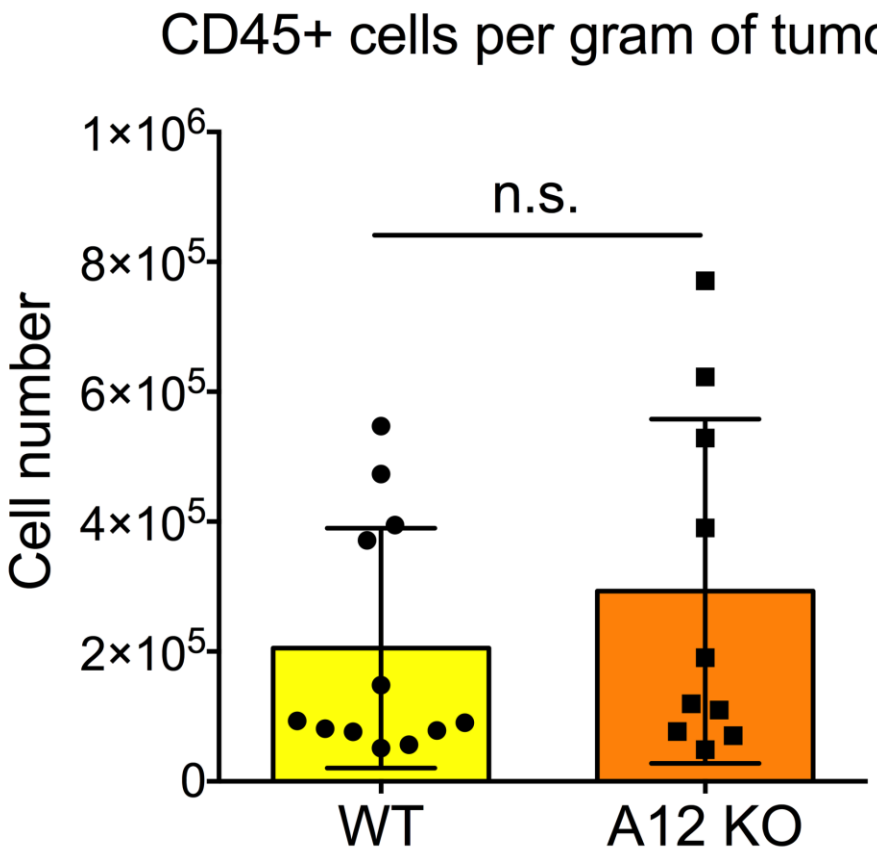

Figure 3.5 Absolute count of leukocytes per gram of T11 tumor

Wild-type or ADAM12 KO T11 cells (1 x 10^4 cells) were orthotopically injected into Balb/cJ mice. Tumors were harvested when their size reached ~100 mm^2 or after 28 days and weighted (WT n=12, ADAM12 KO n=10). Tumor-infiltrating lymphocytes were isolated, labeled with anti-CD45+ antibody, and analyzed by flow cytometry. To obtain absolute cell numbers of CD45+ cells per gram of tumor tissue, known amounts of fluorescent Precision Count Beads™ were added to each sample. Shown are mean values ± S.D. Each point represents a single tumor, in a different mouse. Statistical significance was determined by parametric unpaired t-test. P value < 0.05 was considered significant; n.s., non-significant.

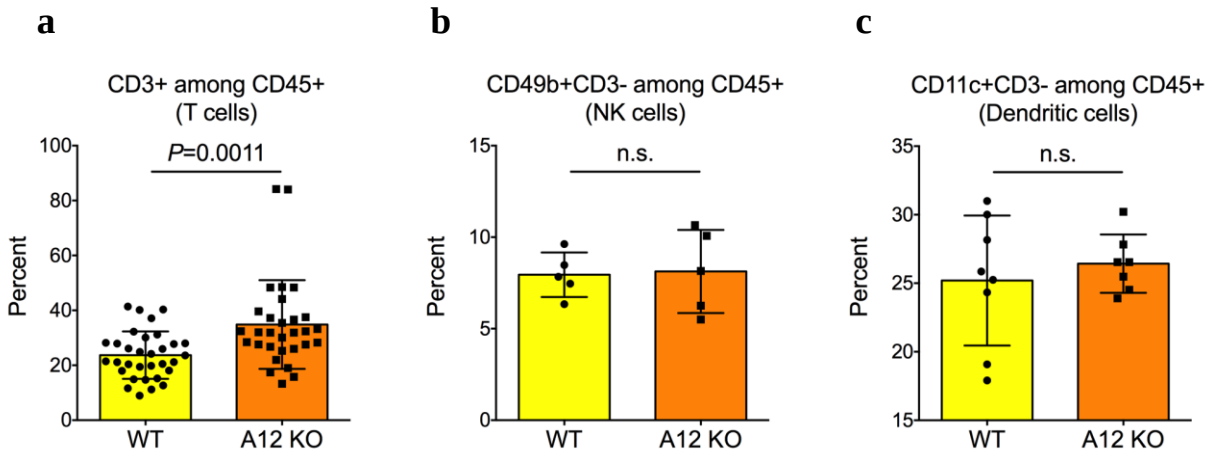

Figure 3.6 Percent of T cells, NK cells and dendritic cells among tumor-infiltrating leukocytes

Wild-type or ADAM12 KO T11 cells (1 x 10^4 cells) were orthotopically injected into Balb/cJ mice. Tumors were harvested when their size reached ~100 mm^2 or after 28 days. Tumor-infiltrating lymphocytes were isolated, labeled with antibodies against the indicated cell surface markers, and analyzed by flow cytometry. **a.)** The frequency of CD3+ T cells among CD45+ cells (WT n=30, ADAM12 KO n=28). **b.)** The frequency of CD49b+CD3- NK cells among CD45+ cells (WT n=5, ADAM12 KO n=5). **c.)** The frequency of CD11c+CD3- dendritic cells among CD45+ cells (WT n=8, ADAM12 KO n=7). Shown are mean values ± S.D. Each point represents a single tumor, in a different mouse. Statistical significance was determined by parametric unpaired t-test. P value < 0.05 was considered significant; n.s., non-significant.

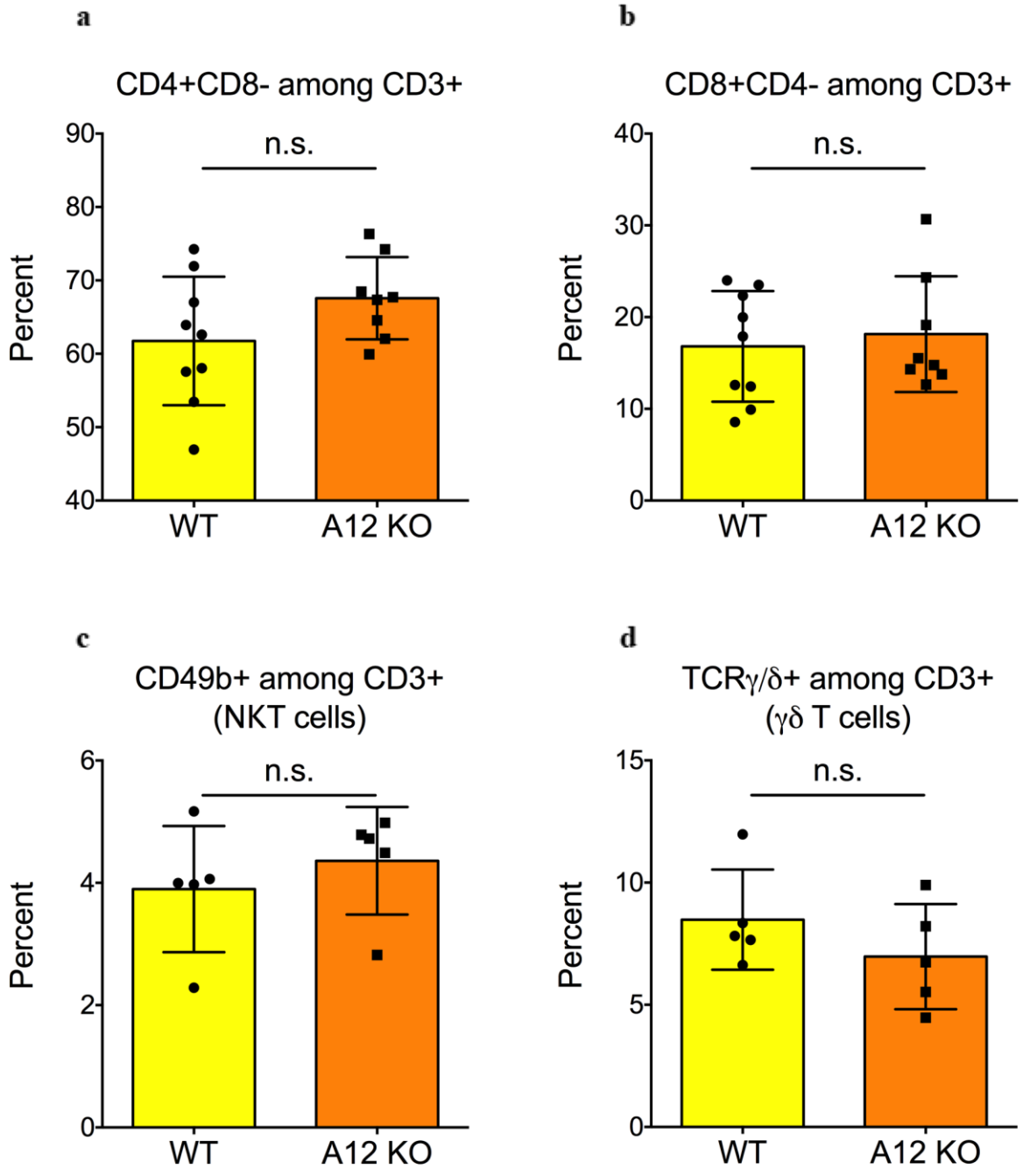

Figure 3.7 Percent of helper T cells, cytotoxic T cells, natural killer T cells and γδ T cells among CD3+ cells

Wild-type or ADAM12 KO T11 cells (1 x 10^4 cells) were orthotopically injected into Balb/cJ mice. Tumors were harvested when their size reached ~100 mm^2 or after 28 days. Tumor-infiltrating lymphocytes were isolated, labeled with antibodies against the indicated cell surface

markers, and analyzed by flow cytometry. **a.)** Percentage of CD4+CD8- T cells among CD3+ cells (WT n=9, ADAM12 KO n=8). **b.)** Percentage of CD8+CD4- cytotoxic T cells among CD3+ cells (WT n=9, ADAM12 KO n=8). **c.)** Percentage of CD49b+ natural killer T cells among CD3+ cells (WT n=5, ADAM12 KO n=5). **d.)** Percentage of TCRγδ+ T cells among CD3+ cells (WT n=5, ADAM12 KO n=5). Shown are mean values ± S.D. Each point represents a single tumor, in a different mouse. Statistical significance determined by parametric unpaired t-test. P value < 0.05 was considered significant; n.s., non-significant.

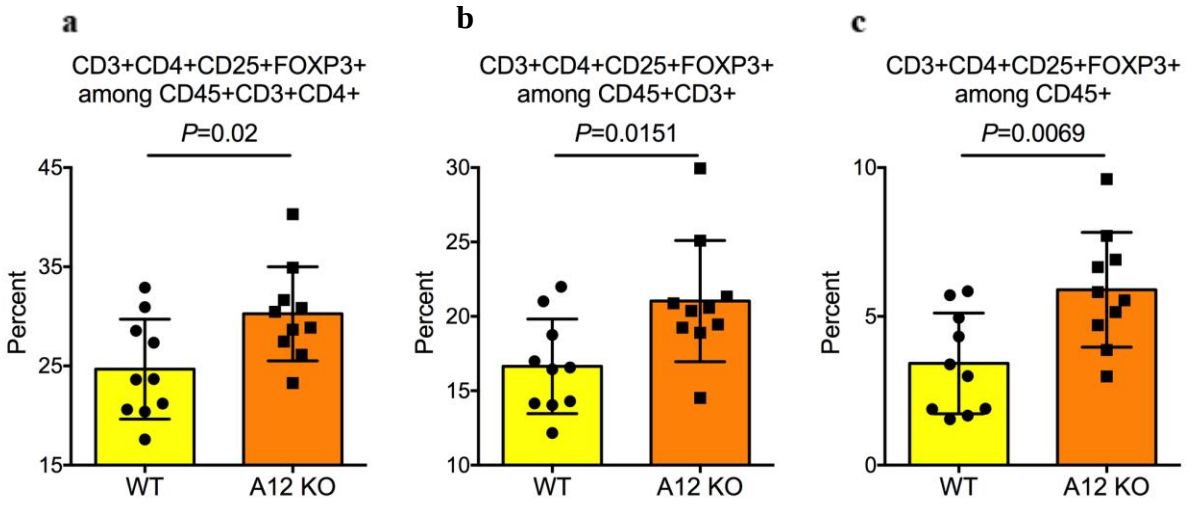

Figure 3.8 Percent of regulatory T cells among CD4+ T cells, all T cells, and all leukocytes. Wild-type or ADAM12 KO T11 cells (1 x 10^4 cells) were orthotopically injected into Balb/cJ mice. Tumors were harvested when their size reached ~100 mm^2 or after 28 days. Tumor-infiltrating lymphocytes were isolated, labeled with antibodies against the indicated cell surface markers, and analyzed by flow cytometry. **a.)** Frequency of CD3+CD4+CD25+FOXP3+ regulatory T cells among CD45+CD3+CD4+ cells (WT n=10, ADAM12 KO n=10). **b.)** Frequency of CD3+CD4+CD25+FOXP3+ regulatory T cells among CD45+CD3+ cells (WT n=10, ADAM12 KO n=10). **c.)** Frequency of CD3+CD4+CD25+FOXP3+ regulatory T cells among CD45+ cells (WT n=10, ADAM12 KO n=10). Shown are mean values ± S.D. Each point represents a single tumor, in a different mouse. Statistical significance determined by parametric unpaired t-test. P value < 0.05 was considered significant.

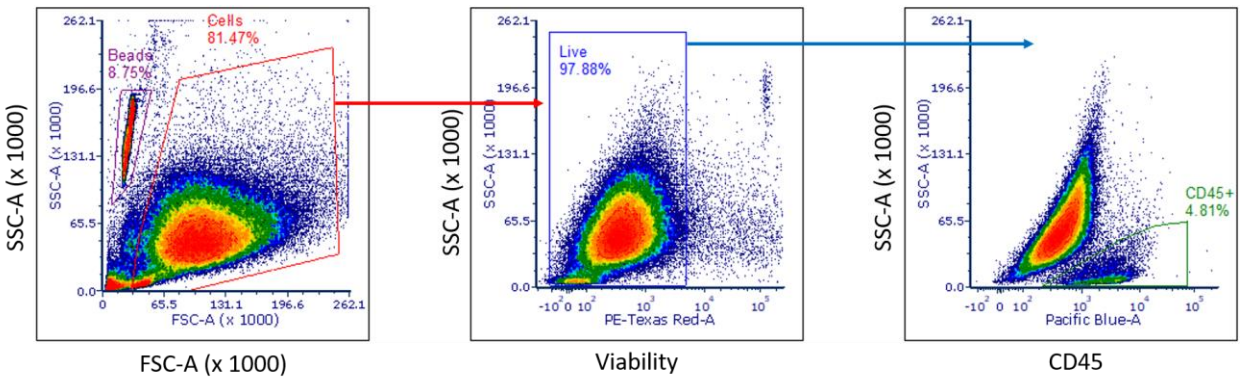

Supplementary Figure 3.1 Gating strategy for the quantification of CD45+ cells shown in Fig. 3.5

Shown is the gating strategy for the flow cytometry analysis of tumor-infiltrating CD45+ leukocytes from ADAM12 KO T11 tumors. Viability dye was propidium iodide.

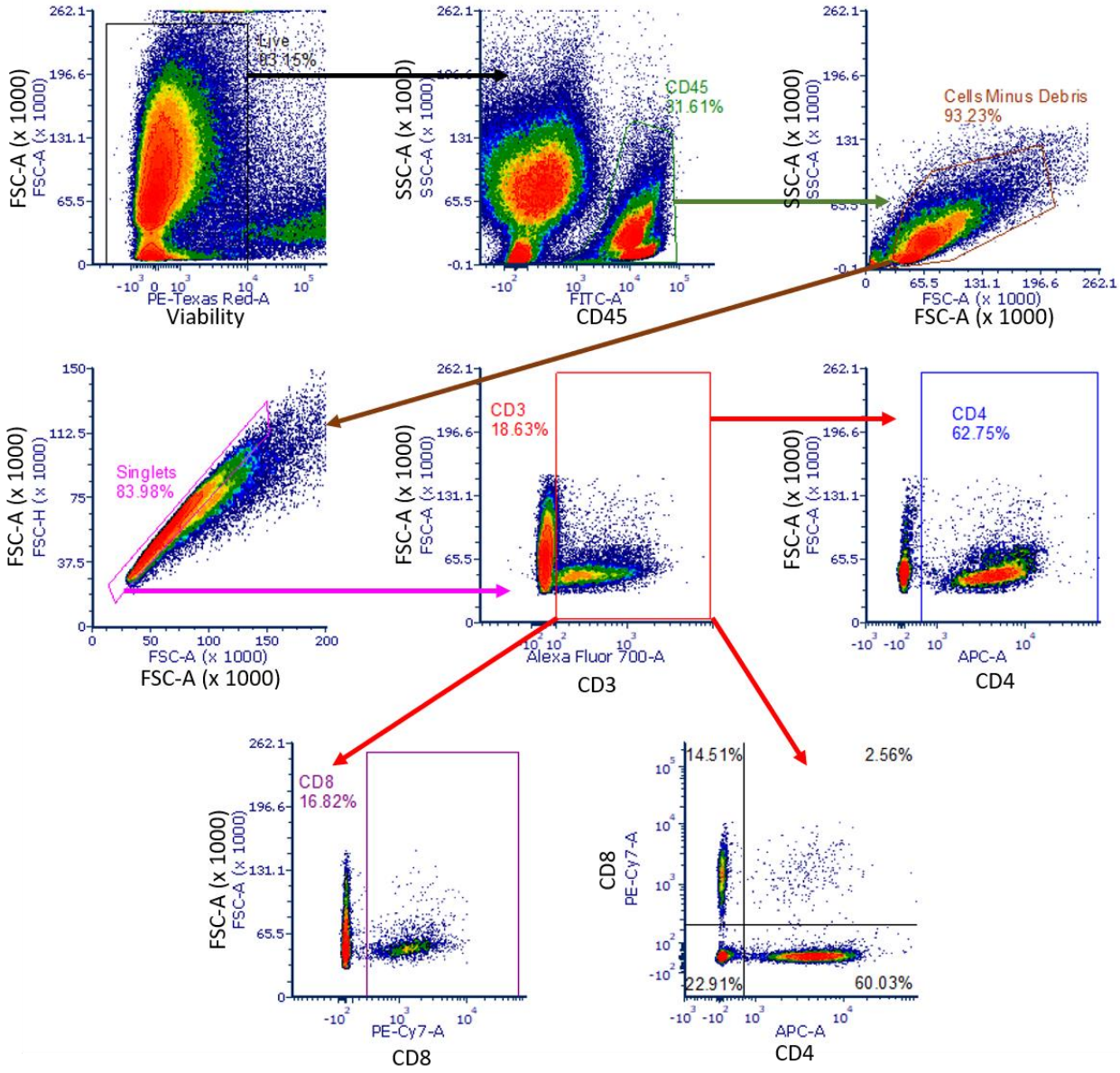

Supplementary Figure 3.2 Gating strategy for the quantification of CD3+, CD4+, or CD8+ cells shown in Fig. 3.6 and 3.7.

Viable CD45+ singlets were gated on CD3 to compute T cells. CD3+ T cells were further gated on CD4 and CD8 to compute CD4+ T cells and cytotoxic T cells, respectively. Viability dye was propidium iodide. Gates were drawn based on fluorescence minus one-controls and isotype controls.

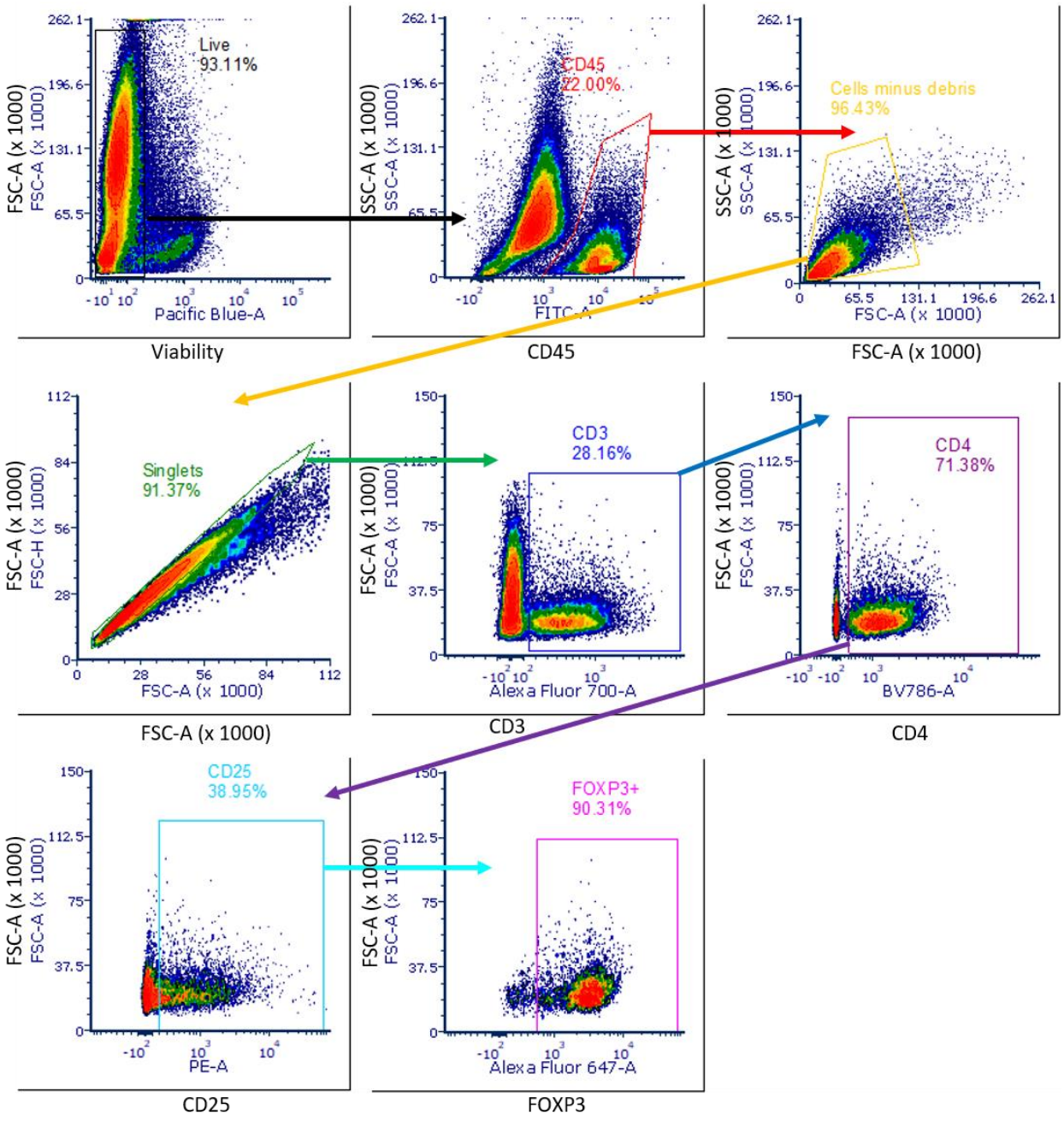

Supplementary Figure 3.3 Gating strategy for the quantification of tumor-infiltrating Tregs shown in Fig. 3.8.

Viable CD45+ singlets were gated on CD3 to compute T cells. CD3+ T cells were further gated on CD4 to compute CD3+CD4+ T cells. CD3+CD4+ T cells were further gated on CD25 and FOXP3 to compute CD25+FOXP3+ regulatory T cells. Fixable Viability Dye eFluor 450 was

used to identify live cells. Gates were drawn based on fluorescence minus one-controls and isotype controls.

Chapter 4 - Conclusions

In this thesis, I investigated PD-L1 and Tregs, two regulators of the tumor immune microenvironment, which have important roles in the immunosuppression in TNBC. PD-L1 is a an immune checkpoint protein which, when bound to the PD-1 receptor, elicits the dulling of T cell responses and immune evasion [12], [13]. Tregs are immunosuppressive cells which suppress the function of immune effector cells through a variety of mechanisms and lead to the tumor immune escape [84], [87]. Together, these regulators play important roles in the progression of TNBC and are promising targets for cancer immunotherapies.

In chapter 2, I investigated the cleavage of PD-L1 on the surface of human triple negative breast cancer cells. We detected the release of a soluble form of PD-L1 from several cultured breast cancer cell lines into the media. We excluded the possibility that the presence of soluble PD-L1 was due to the expression of an alternative mRNA splice variant encoding a soluble protein isoform or due to the release of exosomes harboring transmembrane PD-L1. Next, it was determined that the proteolytic cleavage of PD-L1 generates a ~ 37-kDa N-terminal fragment that accumulates in the media and an 18-kDa C-terminal fragment that remains associated with cells but is unstable and eliminated by lysosomal degradation. This is significant because proteolytic processing of PD-L1 had not yet been described in breast cancer. Most importantly, I identified ADAM10 and ADAM17 as two enzymes mediating the cleavage of transmembrane PD-L1 using pharmacological inhibitors or siRNA-mediated downregulation of ADAM10/17 expression. Because ADAM10 and ADAM17 expression is not exclusive to breast cancer, we also investigated whether these two ADAMs could cleave PD-L1 in other types of cancer cells. Interestingly, we determined that ADAM10 and ADAM17 also mediate the cleavage of PD-L1

in prostate and lung cancer cells. Yet to be determined is the site at which these ADAMs cleave PD-L1 and the effect PD-L1 cleavage has on its suppressive role in the TIME.

In chapter 3, I examined the relationship between ADAM12 and Treg accumulation in the TIME of claudin-low breast tumors. Increased accumulation of Tregs in claudin-low cancers has been linked to poor response rates to immune checkpoint blockade therapies [20]. Currently, the mechanisms of Treg accumulation in the TIME of claudin-low tumors are not well understood. To explore whether there is a direct link between the level of ADAM12 expression in claudin-low breast cancer cells and the abundance of Tregs in the TIME, we first developed an ADAM12-deficient T11 cell line using the CRISPR-Cas9 approach. ADAM12 knockout was confirmed by Western blotting. When ADAM12-deficient T11 cells were injected into the mammary glands of Balb/cJ mice, tumors grew at slower rates than wild-type tumors, but this effect was most likely related to cell-autonomous effects of ADAM12 KO, and not related to the anti-tumor immunity. Importantly, I found an increase in the percent of CD3+ T cells among CD45+ leukocyte cells in ADAM12 KO tumors, and showed an increased frequency of Tregs among CD4+ T cells, T cells and leukocytes in ADAM12 KO tumors. These finding are significant because they establish a cause-and-effect relationship between Treg accumulation and ADAM12 expression and open the door for the development of novel anti-Treg treatments to enhance response rates of immune checkpoint blockade therapies.

Collectively, these results provide insight into the intricate regulatory roles that PD-L1 and Tregs play in the breast cancer TIME and offer novel information that can be useful in the treatment of TNBC. However, there are still numerous questions to be answered about the immunosuppressive roles of PD-L1 and Tregs in breast cancer. For example, it is yet to be determined whether soluble PD-L1 is involved in the dulling of anti-cancer T cell responses or if

it improves anti-tumor immunity. Likewise, an important question remains about the mechanisms by which ADAM12 affects Treg accumulation in the TIME of claudin-low breast cancer. Only by performing further studies and by addressing these unanswered questions can we clarify the clinical implications of the findings presented in this thesis.

References

[1] J. D. C. Hon *et al.*, "Breast cancer molecular subtypes: From TNBC to QNBC," *American Journal of Cancer Research*, vol. 6, no. 9. E-Century Publishing Corporation, pp. 1864–1872, 2016.

[2] J.-R. Jhan, E. R. Andrechek, and E. Andrechek, "Triple-negative breast cancer and the potential for targeted therapy," *Pharmacogenomics*, vol. 18, no. 17, pp. 1595–1609, 2017.

[3] M. A. Medina *et al.*, "Triple-negative breast cancer: A review of conventional and advanced therapeutic strategies," *International Journal of Environmental Research and Public Health*, vol. 17, no. 6. MDPI AG, p. 2078, 01-Mar-2020.

[4] H. G. Russnes, O. C. Lingjærde, A. L. Børresen-Dale, and C. Caldas, "Breast Cancer Molecular Stratification: From Intrinsic Subtypes to Integrative Clusters," *American Journal of Pathology*, vol. 187, no. 10. Elsevier Inc., pp. 2152–2162, 01-Oct-2017.

[5] A. Prat *et al.*, "Clinical implications of the intrinsic molecular subtypes of breast cancer," *Breast*, vol. 24, pp. S26–S35, Nov. 2015.

[6] A. Prat and C. M. Perou, "Deconstructing the molecular portraits of breast cancer," *Mol. Oncol.*, vol. 5, no. 1, pp. 5–23, 2010.

[7] K. Dias *et al.*, "Claudin-Low Breast Cancer; Clinical & Pathological Characteristics," 2017.

[8] "Tumor-Infiltrating Immune Cell Markers (Human) | Cell Signaling Technology." [Online]. Available: https://www.cellsignal.com/contents/science-cst-pathways-immunology-inflammation/tumor-infiltrating-immune-cell-markers-(human)/pathways-ti-icm-human. [Accessed: 16-Sep-2020].

[9] G. Bindea *et al.*, "Spatiotemporal dynamics of intratumoral immune cells reveal the

immune landscape in human cancer," *Immunity*, vol. 39, no. 4, pp. 782–795, Oct. 2013.

[10] M. Binnewies *et al.*, "Understanding the tumor immune microenvironment (TIME) for effective therapy," 2018.

[11] X. Wu *et al.*, "Application of PD-1 Blockade in Cancer Immunotherapy," *Computational and Structural Biotechnology Journal*, vol. 17. Elsevier B.V., pp. 661–674, 01-Jan-2019.

[12] Y. Han, D. Liu, and L. Li, "PD-1/PD-L1 pathway: current researches in cancer.," *Am. J. Cancer Res.*, vol. 10, no. 3, pp. 727–742, 2020.

[13] F. Schütz, S. Stefanovic, L. Mayer, A. Von Au, C. Domschke, and C. Sohn, "PD-1/PD-L1 Pathway in Breast Cancer," *Oncology Research and Treatment*, vol. 40, no. 5. pp. 294–297, 2017.

[14] S. Sakaguchi, T. Yamaguchi, T. Nomura, and M. Ono, "Regulatory T Cells and Immune Tolerance," *Cell*, vol. 133, no. 5. pp. 775–787, 30-May-2008.

[15] D. A. A. Vignali, L. W. Collison, and C. J. Workman, "How regulatory T cells work," *Nature Reviews Immunology*, vol. 8, no. 7. NIH Public Access, pp. 523–532, Jul-2008.

[16] M. García-Aranda and M. Redondo, "Immunotherapy: A challenge of breast cancer treatment," *Cancers (Basel).*, vol. 11, no. 12, Dec. 2019.

[17] "Breast Cancer Immunotherapy - Cancer Research Institute (CRI)." [Online]. Available: https://www.cancerresearch.org/immunotherapy/cancer-types/breast-cancer. [Accessed: 16-Sep-2020].

[18] A. C. Mirando *et al.*, "Regulation of the tumor immune microenvironment and vascular normalization in TNBC murine models by a novel peptide," 2020.

[19] Y. Yang, "Cancer immunotherapy: Harnessing the immune system to battle cancer," *Journal of Clinical Investigation*, vol. 125, no. 9. American Society for Clinical

Investigation, pp. 3335–3337, 01-Sep-2015.

[20] N. A. Taylor *et al.*, “Treg depletion potentiates checkpoint inhibition in claudin-low breast cancer,” *J. Clin. Invest.*, vol. 127, no. 9, pp. 3472–3483, Sep. 2017.

[21] A. Noël *et al.*, “New and paradoxical roles of matrix metalloproteinases in the tumor microenvironment,” *Front. Pharmacol.*, vol. 3 JUL, no. May 2014, 2012.

[22] H. Nagase, R. Visse, and G. Murphy, “Structure and function of matrix metalloproteinases and TIMPs,” *Cardiovasc. Res.*, vol. 69, no. 3, pp. 562–573, Feb. 2006.

[23] D. F. Seals and S. A. Courtneidge, “The ADAMs family of metalloproteases: Multidomain proteins with multiple functions,” *Genes and Development*, vol. 17, no. 1. Cold Spring Harbor Laboratory Press, pp. 7–30, 01-Jan-2003.

[24] M. Mullooly, P. M. McGowan, J. Crown, and M. J. Duffy, “The ADAMs family of proteases as targets for the treatment of cancer,” *Cancer Biology and Therapy*, vol. 17, no. 8. Taylor and Francis Inc., pp. 870–880, 02-Aug-2016.

[25] S. F. Lichtenthaler, M. K. Lemberg, and R. Fluhrer, “Proteolytic ectodomain shedding of membrane proteins in mammals—hardware, concepts, and recent developments,” *EMBO J.*, vol. 37, no. 15, p. 99456, Aug. 2018.

[26] B. Publishing Asia, S. Mochizuki, and Y. Okada, “ADAMs in cancer cell proliferation and progression,” *Cancer Sci*, vol. 98, no. 5, pp. 621–628, 2007.

[27] U. M. Wewer, R. Albrechtsen, and E. Engvall, “ADAM12,” in *The ADAM Family of Proteases*, Springer-Verlag, 2006, pp. 123–146.

[28] J. Wei, B. Richbourgh, T. Jia, and C. Liu, “ADAMTS-12: A multifaced metalloproteinase in arthritis and inflammation,” *Mediators of Inflammation*, vol. 2014. Hindawi Publishing Corporation, 2014.

[29] S. Duhachek-Muggy *et al.*, “Metalloprotease-disintegrin ADAM12 actively promotes the stem cell-like phenotype in claudin-low breast cancer,” *Mol. Cancer*, vol. 16, no. 1, pp. 1–18, Feb. 2017.

[30] S. Shao, Z. Li, W. Gao, G. Yu, D. Liu, and F. Pan, “ADAM-12 as a diagnostic marker for the proliferation, migration and invasion in patients with small cell lung cancer,” *PLoS One*, vol. 9, no. 1, p. 85936, Jan. 2014.

[31] E. Dyczynska, D. Sun, H. Yi, A. Sehara-Fujisawa, C. P. Blobel, and A. Zolkiewska, “Proteolytic processing of delta-like 1 by ADAM proteases,” *J. Biol. Chem.*, vol. 282, no. 1, pp. 436–444, Jan. 2007.

[32] E. Solomon, H. Li, S. D. Muggy, E. Syta, and A. Zolkiewska, “The role of SnoN in transforming growth factor β1-induced expression of metalloprotease-disintegrin ADAM12,” *J. Biol. Chem.*, vol. 285, no. 29, pp. 21969–21977, Jul. 2010.

[33] H. Li, E. Solomon, S. D. Muggy, D. Sun, and A. Zolkiewska, “Metalloprotease-disintegrin ADAM12 expression is regulated by Notch signaling via microRNA-29,” *J. Biol. Chem.*, vol. 286, no. 24, pp. 21500–21510, Jun. 2011.

[34] S. Duhachek-Muggy and A. Zolkiewska, “ADAM12-L is a direct target of the miR-29 and miR-200 families in breast cancer,” *BMC Cancer*, vol. 15, no. 1, p. 93, Dec. 2015.

[35] S. Duhachek-Muggy and A. Zolkiewska, “Abstract B133: Metalloprotease-disintegrin ADAM12-L in breast cancer cells: Regulation of expression by microRNA-200b/c,” in *Molecular Cancer Research*, 2013, vol. 11, no. 10 Supplement, pp. B133–B133.

[36] H. Li, S. Duhachek-Muggy, S. Dubnicka, and A. Zolkiewska, “Metalloproteinase-disintegrin ADAM12 is associated with a breast tumor-initiating cell phenotype,” *Breast Cancer Res. Treat.*, vol. 139, no. 3, pp. 691–703, Jun. 2013.

[37] M. Kveiborg *et al.*, “A role for ADAM12 in breast tumor progression and stromal cell apoptosis,” *Cancer Res.*, vol. 65, no. 11, pp. 4754–4761, Jun. 2005.

[38] R. Roy, U. M. Wewer, D. Zurakowski, S. E. Pories, and M. A. Moses, “ADAM 12 cleaves extracellular matrix proteins and correlates with cancer status and stage,” *J. Biol. Chem.*, vol. 279, no. 49, pp. 51323–51330, Dec. 2004.

[39] S. C. Wei, C. R. Duffy, and J. P. Allison, “fundamental Mechanisms of Immune Checkpoint Blockade Therapy,” *CANCER Discov.*, p. 1069, 2018.

[40] L. A. Emens, “Breast Cancer Immunotherapy: Facts and Hopes,” *Clin Cancer Res*, vol. 24, no. 3, 2018.

[41] M. Sobral-Leite *et al.*, “Assessment of PD-L1 expression across breast cancer molecular subtypes, in relation to mutation rate, BRCA1-like status, tumor-infiltrating immune cells and survival,” 2018.

[42] E. A. Mittendorf *et al.*, “PD-L1 Expression in Triple-Negative Breast Cancer,” *Cancer Immunol. Res.*, vol. 2, no. 4, pp. 361–370, Apr. 2014.

[43] S. Adams *et al.*, “Pembrolizumab monotherapy for previously untreated, PD-L1-positive, metastatic triple-negative breast cancer: Cohort B of the phase II KEYNOTE-086 study,” *Ann. Oncol.*, vol. 30, no. 3, pp. 405–411, Mar. 2019.

[44] L. Y. Dirix *et al.*, “Avelumab, an anti-PD-L1 antibody, in patients with locally advanced or metastatic breast cancer: a phase 1b JAVELIN Solid Tumor study,” *Breast Cancer Res. Treat.*, vol. 167, pp. 671–686, 2018.

[45] P. Schmid *et al.*, “Atezolizumab and nab-paclitaxel in advanced triple-negative breast cancer,” *N. Engl. J. Med.*, vol. 379, no. 22, pp. 2108–2121, Nov. 2018.

[46] I. Zerdes, A. Matikas, J. Bergh, G. Z. Rassidakis, and T. Foukakis, “Genetic,

transcriptional and post-translational regulation of the programmed death protein ligand 1 in cancer: biology and clinical correlations," *Oncogene*, vol. 37, no. 34. Nature Publishing Group, pp. 4639–4661, 23-Aug-2018.

[47] H. Horita, A. Law, S. Hong, and K. Middleton, "Identifying Regulatory Posttranslational Modifications of PD-L1: A Focus on Monoubiquitinaton," *Neoplasia (United States)*, vol. 19, no. 4, pp. 346–353, Apr. 2017.

[48] C. W. Li *et al.*, "Glycosylation and stabilization of programmed death ligand-1 suppresses T-cell activity," *Nat. Commun.*, vol. 7, Aug. 2016.

[49] Y. Yang *et al.*, "Palmitoylation stabilizes PD-L1 to promote breast tumor growth," *Cell Research*, vol. 29, no. 1. Nature Publishing Group, pp. 83–86, 01-Jan-2019.

[50] M. L. Burr *et al.*, "CMTM6 maintains the expression of PD-L1 and regulates anti-Tumour immunity," *Nature*, vol. 549, no. 7670, pp. 101–105, Sep. 2017.

[51] R. Mezzadra *et al.*, "Identification of CMTM6 and CMTM4 as PD-L1 protein regulators," *Nature*, vol. 549, no. 7670, pp. 106–110, Sep. 2017.

[52] T. L. Whiteside, "Exosomes and tumor-mediated immune suppression," *Journal of Clinical Investigation*, vol. 126, no. 4. American Society for Clinical Investigation, pp. 1216–1223, 01-Apr-2016.

[53] M. Poggio *et al.*, "Suppression of Exosomal PD-L1 Induces Systemic Anti-tumor Immunity and Memory," *Cell*, vol. 177, no. 2, pp. 414-427.e13, Apr. 2019.

[54] J. Zhou *et al.*, "Soluble PD-L1 as a biomarker in malignant melanoma treated with checkpoint blockade," *Cancer Immunol. Res.*, vol. 5, no. 6, pp. 480–492, Jun. 2017.

[55] K. M. Mahoney *et al.*, "A secreted PD-L1 splice variant that covalently dimerizes and mediates immunosuppression," *Cancer Immunol. Immunother.*, vol. 68, no. 3, pp. 421–

432, Mar. 2019.

[56] X. Frigola *et al.*, “Identification of a soluble form of B7-H1 that retains immunosuppressive activity and is associated with aggressive renal cell carcinoma,” *Clin. Cancer Res.*, vol. 17, no. 7, pp. 1915–1923, Apr. 2011.

[57] C. Dezutter-Dambuyant *et al.*, “A novel regulation of PD-1 ligands on mesenchymal stromal cells through MMP-mediated proteolytic cleavage,” *Oncoimmunology*, vol. 5, no. 3, Mar. 2016.

[58] L. C. Davies, N. Heldring, N. Kadri, and K. Le Blanc, “Mesenchymal Stromal Cell Secretion of Programmed Death-1 Ligands Regulates T Cell Mediated Immunosuppression,” *Stem Cells*, vol. 35, no. 3, pp. 766–776, Mar. 2017.

[59] M. Hira-Miyazawa *et al.*, “Regulation of programmed-death ligand in the human head and neck squamous cell carcinoma microenvironment is mediated through matrix metalloproteinase-mediated proteolytic cleavage,” *Int. J. Oncol.*, vol. 52, no. 2, pp. 379–388, Feb. 2018.

[60] S. Weber and P. Saftig, “Ectodomain shedding and ADAMs in development,” *Development (Cambridge)*, vol. 139, no. 20. Oxford University Press for The Company of Biologists Limited, pp. 3693–3709, 15-Oct-2012.

[61] R. Marcotte *et al.*, “Functional Genomic Landscape of Human Breast Cancer Drivers, Vulnerabilities, and Resistance,” *Cell*, vol. 164, no. 1–2, pp. 293–309, Jan. 2016.

[62] A. Daemen *et al.*, “Modeling precision treatment of breast cancer,” *Genome Biol.*, vol. 14, no. 10, Dec. 2013.

[63] A. Garcia-Diaz *et al.*, “Interferon Receptor Signaling Pathways Regulating PD-L1 and PD-L2 Expression,” *Cell Rep.*, vol. 29, no. 11, p. 3766, Dec. 2019.

[64] R. Xu, R. J. Simpson, and D. W. Greening, “A protocol for isolation and proteomic characterization of distinct extracellular vesicle subtypes by sequential centrifugal ultrafiltration,” in *Methods in Molecular Biology*, vol. 1545, Humana Press Inc., 2017, pp. 91–116.

[65] Y. Chen *et al.*, “Development of a sandwich ELISA for evaluating soluble PD-L1 (CD274) in human sera of different ages as well as supernatants of PD-L1 + cell lines,” *Cytokine*, vol. 56, no. 2, pp. 231–238, Nov. 2011.

[66] A. Ludwig *et al.*, “Metalloproteinase Inhibitors for the Disintegrin-Like Metalloproteinases ADAM10 and ADAM17 that Differentially Block Constitutive and Phorbol Ester-Inducible Shedding of Cell Surface Molecules,” *Comb. Chem. High Throughput Screen.*, vol. 8, no. 2, pp. 161–171, Mar. 2005.

[67] M. L. Moss and F. H. Rasmussen, “Fluorescent substrates for the proteinases ADAM17, ADAM10, ADAM8, and ADAM12 useful for high-throughput inhibitor screening,” *Anal. Biochem.*, vol. 366, no. 2, pp. 144–148, Jul. 2007.

[68] K. Horiuchi *et al.*, “Substrate selectivity of epidermal growth factor-receptor ligand sheddases and their regulation by phorbol esters and calcium influx,” *Mol. Biol. Cell*, vol. 18, no. 1, pp. 176–188, Jan. 2007.

[69] S. M. Le Gall *et al.*, “ADAMs 10 and 17 Represent Differentially Regulated Components of a General Shedding Machinery for Membrane Proteins Such as Transforming Growth Factor , L-Selectin, and Tumor Necrosis Factor,” *Mol. Biol. Cell*, vol. 20, pp. 1785–1794, 2009.

[70] J. Vandooren, P. E. Van Den Steen, and G. Opdenakker, “Biochemistry and molecular biology of gelatinase B or matrix metalloproteinase-9 (MMP-9): The next decade,”

Critical Reviews in Biochemistry and Molecular Biology, vol. 48, no. 3. Informa Healthcare, pp. 222–272, 2013.

[71] B. N. Lambrecht, M. Vanderkerken, and H. Hammad, "The emerging role of ADAM metalloproteinases in immunity," *Nature Reviews Immunology*, vol. 18, no. 12. Nature Publishing Group, pp. 745–758, 01-Dec-2018.

[72] F. Zunke and S. Rose-John, "The shedding protease ADAM17: Physiology and pathophysiology," *Biochimica et Biophysica Acta - Molecular Cell Research*, vol. 1864, no. 11. Elsevier B.V., pp. 2059–2070, 01-Nov-2017.

[73] Y. Jing *et al.*, "Identification of an ADAM17 Cleavage Region in Human CD16 (FcγRIII) and the Engineering of a Non-Cleavable Version of the Receptor in NK Cells," *PLoS One*, vol. 10, no. 3, p. e0121788, Mar. 2015.

[74] N. Li *et al.*, "Metalloproteases regulate T-cell proliferation and effector function via LAG-3," *EMBO J.*, vol. 26, no. 2, pp. 494–504, Jan. 2007.

[75] S. Fabre-Lafay, S. Garrido-Urbani, N. Reymond, A. Gonçalves, P. Dubreuil, and M. Lopez, "Nectin-4, a new serological breast cancer marker, is a substrate for tumor necrosis factor-α-converting enzyme (TACE)/ADAM-17," *J. Biol. Chem.*, vol. 280, no. 20, pp. 19543–19550, May 2005.

[76] L. Wartosch, U. Günesdogan, S. C. Graham, and J. P. Luzio, "Recruitment of VPS33A to HOPS by VPS16 Is Required for Lysosome Fusion with Endosomes and Autophagosomes," *Traffic*, vol. 16, no. 7, pp. 727–742, Jul. 2015.

[77] Z. Liang *et al.*, "High-affinity human PD-L1 variants attenuate the suppression of T cell activation," *Oncotarget*, vol. 8, no. 51, pp. 88360–88375, Oct. 2017.

[78] M. J. Butte, M. E. Keir, T. B. Phamduy, A. H. Sharpe, and G. J. Freeman, "Programmed

Death-1 Ligand 1 Interacts Specifically with the B7-1 Costimulatory Molecule to Inhibit T Cell Responses," *Immunity*, vol. 27, no. 1, pp. 111–122, Jul. 2007.

[79] A. Chaudhri, Y. Xiao, A. N. Klee, X. Wang, B. Zhu, and G. J. Freeman, "PD-L1 Binds to B7-1 only in cis on the same cell surface," *Cancer Immunol. Res.*, vol. 6, no. 8, pp. 921–929, Aug. 2018.

[80] D. Sugiura *et al.*, "Restriction of PD-1 function by cis-PD-L1/CD80 interactions is required for optimal T cell responses," *Science (80-.).*, vol. 364, no. 6440, pp. 558–566, 2019.

[81] Y. Zhao, D. L. Harrison, Y. Song, J. Ji, J. Huang, and E. Hui, "Antigen-Presenting Cell-Intrinsic PD-1 Neutralizes PD-L1 in cis to Attenuate PD-1 Signaling in T Cells," *Cell Rep.*, vol. 24, no. 2, pp. 379-390.e6, Jul. 2018.

[82] L. Chen and D. B. Flies, "Molecular mechanisms of T cell co-stimulation and co-inhibition," *Nature Reviews Immunology*, vol. 13, no. 4. Nature Publishing Group, pp. 227–242, 08-Apr-2013.

[83] A. Prat *et al.*, "Phenotypic and molecular characterization of the claudin-low intrinsic subtype of breast cancer," *Breast Cancer Res.*, vol. 12, no. 5, p. R68, Sep. 2010.

[84] Y. Ohue and H. Nishikawa, "Regulatory T (Treg) cells in cancer: Can Treg cells be a new therapeutic target?," *Cancer Science*, vol. 110, no. 7. Blackwell Publishing Ltd, pp. 2080–2089, 01-Jul-2019.

[85] H. Li *et al.*, "An essential role of metalloprotease-disintegrin ADAM12 in triple-negative breast cancer," *Breast Cancer Res. Treat.*, vol. 135, no. 3, pp. 759–769, Oct. 2012.

[86] J. Usary, D. B. Darr, A. Pfefferle, and C. M. Perou, "Genetically Engineered Mouse Models of Distinct Breast Cancer Subtypes."

[87] C. Li, P. Jiang, S. Wei, X. Xu, and J. Wang, “Regulatory T cells in tumor microenvironment: New mechanisms, potential therapeutic strategies and future prospects,” *Molecular Cancer*, vol. 19, no. 1. BioMed Central, p. 116, 17-Jul-2020.

Appendix A - Copyright Permissions

SPRINGER NATURE LICENSE
TERMS AND CONDITIONS
Oct 12, 2020

This Agreement between Mrs. Yeni Romero ("You") and Springer Nature ("Springer Nature") consists of your license details and the terms and conditions provided by Springer Nature and Copyright Clearance Center.

License Number	4926491456472
License date	Oct 12, 2020
Licensed Content Publisher	Springer Nature
Licensed Content Publication	Cancer Immunology, Immunotherapy
Licensed Content Title	Proteolytic processing of PD-L1 by ADAM proteases in breast cancer cells
Licensed Content Author	Yeni Romero et al
Licensed Content Date	Dec 3, 2019
Type of Use	Thesis/Dissertation
Requestor type	academic/university or research institute
Format	electronic
Portion	full article/chapter
Will you be translating?	no
Circulation/distribution	1 - 29
Author of this Springer Nature content	yes
Title	Regulators of the Breast Tumor Immune Microenvironment: PD-L1 and Regulatory T Cells
Institution name	Kansas State University
Expected presentation date	Oct 2020
Order reference number	1090
Requestor Location	Mrs. Yeni Romero 2017 Hillview Drive MANHATTAN, KS 66502 United States Attn: Yeni Romero
Total	0.00 USD
Terms and Conditions	

Springer Nature Customer Service Centre GmbH
Terms and Conditions

This agreement sets out the terms and conditions of the licence (the **Licence**) between you and **Springer Nature Customer Service Centre GmbH** (the **Licensor**). By clicking 'accept' and completing the transaction for the material (**Licensed Material**), you also confirm your acceptance of these terms and conditions.

1. **Grant of License**

    1. The Licensor grants you a personal, non-exclusive, non-transferable, world-wide licence to reproduce the Licensed Material for the purpose specified in your order only. Licences are granted for the specific use requested in the order and for no other use, subject to the conditions below.

    2. The Licensor warrants that it has, to the best of its knowledge, the rights to license reuse of the Licensed Material. However, you should ensure that the material you are requesting is original to the Licensor and does not carry the copyright of another entity (as credited in the published version).

    3. If the credit line on any part of the material you have requested indicates that it was reprinted or adapted with permission from another source, then you should also seek permission from that source to reuse the material.

2. **Scope of Licence**

    1. You may only use the Licensed Content in the manner and to the extent permitted by these Ts&Cs and any applicable laws.

    2. A separate licence may be required for any additional use of the Licensed Material, e.g. where a licence has been purchased for print only use, separate permission must be obtained for electronic re-use. Similarly, a licence is only valid in the language selected and does not apply for editions in other languages unless additional translation rights have been granted separately in the licence. Any content owned by third parties are expressly excluded from the licence.

    3. Similarly, rights for additional components such as custom editions and derivatives require additional permission and may be subject to an additional fee. Please apply to Journalpermissions@springernature.com/bookpermissions@springernature.com for these rights.

    4. Where permission has been granted **free of charge** for material in print, permission may also be granted for any electronic version of that work, provided

that the material is incidental to your work as a whole and that the electronic version is essentially equivalent to, or substitutes for, the print version.

5. An alternative scope of license may apply to signatories of the STM Permissions Guidelines, as amended from time to time.

Duration of Licence

1. A licence for is valid from the date of purchase ('Licence Date') at the end of the relevant period in the below table:

Scope of Licence	Duration of Licence
Post on a website	12 months
Presentations	12 months
Books and journals	Lifetime of the edition in the language purchased

Acknowledgement

1. The Licensor's permission must be acknowledged next to the Licenced Material in print. In electronic form, this acknowledgement must be visible at the same time as the figures/tables/illustrations or abstract, and must be hyperlinked to the journal/book's homepage. Our required acknowledgement format is in the Appendix below.

Restrictions on use

1. Use of the Licensed Material may be permitted for incidental promotional use and minor editing privileges e.g. minor adaptations of single figures, changes of format, colour and/or style where the adaptation is credited as set out in Appendix 1 below. Any other changes including but not limited to, cropping, adapting, omitting material that affect the meaning, intention or moral rights of the author are strictly prohibited.

2. You must not use any Licensed Material as part of any design or trademark.

3. Licensed Material may be used in Open Access Publications (OAP) before publication by Springer Nature, but any Licensed Material must be removed from OAP sites prior to final publication.

Ownership of Rights

1. Licensed Material remains the property of either Licensor or the relevant third party and any rights not explicitly granted herein are expressly reserved.

Warranty

IN NO EVENT SHALL LICENSOR BE LIABLE TO YOU OR ANY OTHER PARTY OR ANY OTHER PERSON OR FOR ANY SPECIAL, CONSEQUENTIAL, INCIDENTAL OR

INDIRECT DAMAGES, HOWEVER CAUSED, ARISING OUT OF OR IN CONNECTION WITH THE DOWNLOADING, VIEWING OR USE OF THE MATERIALS REGARDLESS OF THE FORM OF ACTION, WHETHER FOR BREACH OF CONTRACT, BREACH OF WARRANTY, TORT, NEGLIGENCE, INFRINGEMENT OR OTHERWISE (INCLUDING, WITHOUT LIMITATION, DAMAGES BASED ON LOSS OF PROFITS, DATA, FILES, USE, BUSINESS OPPORTUNITY OR CLAIMS OF THIRD PARTIES), AND WHETHER OR NOT THE PARTY HAS BEEN ADVISED OF THE POSSIBILITY OF SUCH DAMAGES. THIS LIMITATION SHALL APPLY NOTWITHSTANDING ANY FAILURE OF ESSENTIAL PURPOSE OF ANY LIMITED REMEDY PROVIDED HEREIN.

Limitations

1. ***BOOKS ONLY:***Where **'reuse in a dissertation/thesis'** has been selected the following terms apply: Print rights of the final author's accepted manuscript (for clarity, NOT the published version) for up to 100 copies, electronic rights for use only on a personal website or institutional repository as defined by the Sherpa guideline (www.sherpa.ac.uk/romeo/).

Termination and Cancellation

1. Licences will expire after the period shown in Clause 3 (above).

2. Licensee reserves the right to terminate the Licence in the event that payment is not received in full or if there has been a breach of this agreement by you.

Appendix 1 — Acknowledgements:

For Journal Content:
Reprinted by permission from [**the Licensor**]: [**Journal Publisher** (e.g. Nature/Springer/Palgrave)] [**JOURNAL NAME**] [**REFERENCE CITATION** (Article name, Author(s) Name), [**COPYRIGHT**] (year of publication)
For **Advance Online Publication papers:**
Reprinted by permission from [**the Licensor**]: [**Journal Publisher** (e.g. Nature/Springer/Palgrave)] [**JOURNAL NAME**] [**REFERENCE CITATION** (Article name, Author(s) Name), [**COPYRIGHT**] (year of publication), advance online publication, day month year (doi: 10.1038/sj.[JOURNAL ACRONYM].)
For Adaptations/Translations:
Adapted/Translated by permission from [**the Licensor**]: [**Journal Publisher** (e.g. Nature/Springer/Palgrave)] [**JOURNAL NAME**] [**REFERENCE CITATION** (Article name, Author(s) Name), [**COPYRIGHT**] (year of publication)
Note: For any republication from the British Journal of Cancer, the following credit line style applies:
Reprinted/adapted/translated by permission from [**the Licensor**]: on behalf of Cancer Research UK: : [**Journal Publisher** (e.g. Nature/Springer/Palgrave)] [**JOURNAL NAME**] [**REFERENCE CITATION** (Article name, Author(s) Name), [**COPYRIGHT]** (year of publication)

For **Advance Online Publication** papers:
Reprinted by permission from The [**the Licensor**]: on behalf of Cancer Research UK: [**Journal Publisher** (e.g. Nature/Springer/Palgrave)] [**JOURNAL NAME**] [**REFERENCE CITATION** (Article name, Author(s) Name), [**COPYRIGHT**] (year of publication), advance online publication, day month year (doi: 10.1038/sj.[JOURNAL ACRONYM])

For Book content:
Reprinted/adapted by permission from [**the Licensor**]: [**Book Publisher** (e.g. Palgrave Macmillan, Springer etc) [**Book Title**] by [**Book author**(s)] [**COPYRIGHT**] (year of publication)